The Astrophysical Journal Supplement Series, 227:11 (27pp), 2016 November doi:10.3847/0067-0049/227/1/11

THE PAN-STARRS1 DISTANT $z > 5.6$ QUASAR SURVEY: MORE THAN 100 QUASARS WITHIN THE FIRST GYR OF THE UNIVERSE

E. Bañados[1,2,15], B. P. Venemans[1], R. Decarli[1], E. P. Farina[1], C. Mazzucchelli[1], F. Walter[1], X. Fan[3], D. Stern[4], E. Schlafly[1,5,16], K. C. Chambers[6], H-W. Rix[1], L. Jiang[7], I. McGreer[3], R. Simcoe[8], F. Wang[3,9], J. Yang[3,9], E. Morganson[10], G. De Rosa[11], J. Greiner[12], M. Baloković[13], W. S. Burgett[6], T. Cooper[8], P. W. Draper[14], H. Flewelling[6], K. W. Hodapp[6], H. D. Jun[4], N. Kaiser[6], R.-P. Kudritzki[6], E. A. Magnier[6], N. Metcalfe[14], D. Miller[8], J.-T. Schindler[3], J. L. Tonry[6], R. J. Wainscoat[6], C. Waters[6], and Q. Yang[3,9]

[1] Max Planck Institut für Astronomie, Königstuhl 17, D-69117, Heidelberg, Germany; ebanados@carnegiescience.edu
[2] The Observatories of the Carnegie Institute of Washington, 813 Santa Barbara Street, Pasadena, CA 91101, USA
[3] Steward Observatory, The University of Arizona, 933 North Cherry Avenue, Tucson, AZ 85721–0065, USA
[4] Jet Propulsion Laboratory, California Institute of Technology, 4800 Oak Grove Drive, Pasadena, CA 91109, USA
[5] Lawrence Berkeley National Laboratory, One Cyclotron Road, Berkeley, CA 94720, USA
[6] Institute for Astronomy, University of Hawaii, 2680 Woodlawn Drive, Honolulu, HI 96822, USA
[7] Kavli Institute for Astronomy and Astrophysics, Peking University, Beijing 100871, China
[8] MIT-Kavli Center for Astrophysics and Space Research, 77 Massachusetts Avenue, Cambridge, MA 02139, USA
[9] Department of Astronomy, School of Physics, Peking University, Beijing 100871, China
[10] National Center for Supercomputing Applications, University of Illinois at Urbana-Champaign, 1205 W. Clark Street, Urbana, IL 61801, USA
[11] Space Telescope Science Institute, 3700 San Martin Drive, Baltimore, MD 21218, USA
[12] Max-Planck-Institut für extraterrestrische Physik, Giessenbachstrasse 1, D-85748 Garching, Germany
[13] Cahill Center for Astronomy and Astrophysics, California Institute of Technology, Pasadena, CA 91125, USA
[14] Department of Physics, Durham University, South Road, Durham DH1 3LE, UK
Received 2016 May 27; revised 2016 July 25; accepted 2016 August 3; published 2016 November 14

ABSTRACT

Luminous quasars at $z > 5.6$ can be studied in detail with the current generation of telescopes and provide us with unique information on the first gigayear of the universe. Thus far, these studies have been statistically limited by the number of quasars known at these redshifts. Such quasars are rare, and therefore, wide-field surveys are required to identify them, and multiwavelength data are required to separate them efficiently from their main contaminants, the far more numerous cool dwarfs. In this paper, we update and extend the selection for the $z \sim 6$ quasars presented in Bañados et al. (2014) using the Pan-STARRS1 (PS1) survey. We present the PS1 distant quasar sample, which currently consists of 124 quasars in the redshift range $5.6 \lesssim z \lesssim 6.7$ that satisfy our selection criteria. Of these quasars, 77 have been discovered with PS1, and 63 of them are newly identified in this paper. We present the composite spectra of the PS1 distant quasar sample. This sample spans a factor of ∼20 in luminosity and shows a variety of emission line properties. The number of quasars at $z > 5.6$ presented in this work almost doubles the previously known quasars at these redshifts, marking a transition phase from studies of individual sources to statistical studies of the high-redshift quasar population, which was impossible with earlier, smaller samples.

Key words: cosmology: observations – quasars: emission lines – quasars: general

Supporting material: machine-readable tables

1. INTRODUCTION

Quasars—accreting supermassive black holes in the center of massive galaxies—have fascinated astronomers since their discovery over 50 years ago (Schmidt 1963). The extreme luminosity of quasars makes them light beacons that illuminate our knowledge of the early universe. Within only a few years of their initial discovery, quasars with redshifts as high as $z \sim 2$ (i.e., when the universe was about one quarter of its current age) were already being identified (e.g., Schmidt 1965; Arp et al. 1967). This allowed astronomers to study objects at distances that at the time were unconceivable, expanding our view of the universe.

About fifteen years ago the first quasars at $z > 5.6$ (i.e., within the first gigayear of the universe) were discovered (Fan et al. 2000). By 2011 the number of quasars at $z > 5.6$ had reached 60, with most of the contributions coming from large surveys, such as the SDSS (e.g., Fan et al. 2006; Jiang et al. 2008), CFHQS (e.g., Willott et al. 2007, 2010b), and UKIDSS (e.g., Venemans et al. 2007; Mortlock et al. 2011). Over the last three years a second wave of quasar discoveries has started due to new optical and near-infrared large sky surveys, such as VIKING (Venemans et al. 2013), VST-ATLAS (Carnall et al. 2015), DES (Reed et al. 2015), HSC (Matsuoka et al. 2016), and Pan-STARRS1 (PS1; e.g., Bañados et al. 2014).

Quasars within the first gigayear of the universe place strong constraints on black hole formation models (Volonteri 2012) and are fundamental probes of the final phases of cosmological reionization (see Becker et al. 2015a; Mortlock 2015, for recent reviews). However, the conclusions provided are still fairly weak, due to the low number of quasar sightlines studied so far.

Over the last years, we have been searching for high-redshift quasars in the PS1 survey (Kaiser et al. 2002, 2010), which has imaged the whole sky above a declination of $-30°$ for about four years in five filters ($g_{\rm P1}$, $r_{\rm P1}$, $i_{\rm P1}$, $z_{\rm P1}$, $y_{\rm P1}$). Our efforts have resulted in 14 published quasars at $z > 5.6$ (Morganson et al. 2012; Bañados et al. 2014, 2015b; Venemans et al.

[15] Carnegie-Princeton Fellow.
[16] Hubble Fellow.

2015a), one of which is among the brightest quasars known in the early universe in both UV and [C II] luminosities (Bañados et al. 2015a). In this work we update our selection criteria and present 63 new quasars. The 77 PS1-discovered $z > 5.6$ quasars almost double the previously known number of quasars at these redshifts, giving us the opportunity to perform initial characterizations of the high-redshift quasar population as a whole.

The quasars presented in this paper were selected from the first and second internal releases of the stacked PS1 data (PV1 and PV2, respectively, in the internal naming convention). At the time of writing of this article, the PV3 and final version of the PS1 catalog was made available to us. Therefore, throughout the paper we quote the PV3 PS1 magnitudes corrected for Galactic extinction[17] (Schlafly & Finkbeiner 2011).

This article is organized as follows. In Section 2, we introduce our updated color selection criteria for *i*-dropout $5.7 \lesssim z \lesssim 6.5$ quasars from the PS1 stacked catalog and summarize our candidate selection procedures. The imaging and spectroscopic follow-up observations are presented in Section 3. In Section 4, we show the spectra of the 77 PS1-discovered quasars at $5.7 \lesssim z \lesssim 6.7$ (63 newly discovered in this paper) and discuss some individual objects. In Section 5, we introduce the PS1 distant quasar sample, which currently consists of 124 quasars at $z > 5.6$ that were discovered by PS1 or that satisfy the selection criteria presented in this work or in Venemans et al. (2015a). We create composite spectra from the PS1 distant quasar sample in Section 6 and revisit the discussion of how typical weak-line quasars are at $z \sim 6$ in Section 7. Finally, we summarize our results in Section 8.

The International Astronomical Union naming convention for non-transient objects discovered using the Pan-STARRS1 survey is "PSO JRRR.rrrr+DD.dddd," where RRR.rrrr and +DD.dddd are the right ascension and declination in decimal degrees (J2000), respectively. For PS1-discovered quasars we will use abbreviated names of the form "PRRR+DD," while quasars discovered by other surveys will be named as "Jhhmm+ddmm." Table 7 in the Appendix A lists the coordinates and redshifts of all 173 $z > 5.6$ quasars known to date.[18]

All magnitudes are given in the AB system. When referring to limiting magnitudes ($\mathrm{mag_{P1,lim}}$) throughout the text, these correspond to 3σ-limiting magnitudes. We use a flat ΛCDM cosmology with $H_0 = 67.7\ \mathrm{km\,s^{-1}\ Mpc^{-1}}$, $\Omega_M = 0.307$, and $\Omega_\Lambda = 0.693$ (Planck Collaboration et al. 2016).

2. CANDIDATE SELECTION

The main contaminants of $z \sim 6$–7 quasar searches are brown dwarfs, especially late M, L, and T dwarfs, which can have optical colors similar to quasars' but are much more abundant. Figure 1 shows the expected location of the composite quasar spectrum created in Section 6 in the $i_{\rm P1} - z_{\rm P1}$ versus $z_{\rm P1} - y_{\rm P1}$ color space as its redshift is increased from $z = 5.5$ to $z = 6.5$. In order to visualize the PS1 colors of brown dwarfs, we cross-matched the M dwarf catalog of West et al. (2011) to the PS1 PV3 catalog. We also cross-matched

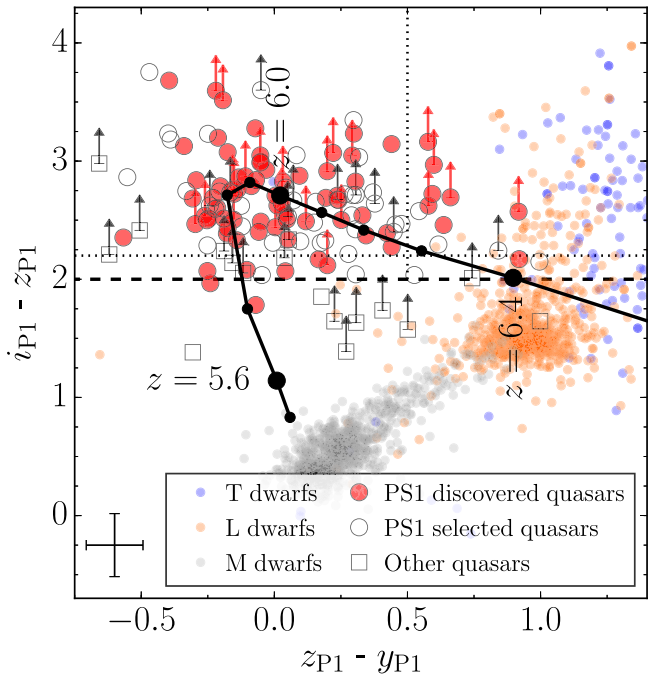

Figure 1. Color–color diagram showing the criteria used to select quasar candidates (dashed and dotted–dashed lines; see text). The thick black line shows the expected color of the PS1 composite quasar spectrum created in Section 6 redshifted from $z = 5.5$ to $z = 6.5$ in steps of $\Delta z = 0.1$. The L/T dwarfs that have a PS1 counterpart are shown with small orange/blue circles. A subsample of the M dwarfs from West et al. (2011) are represented by small gray circles. The upper limits for brown dwarfs are not plotted to enhance the clarity of the figure. The red filled circles are quasars discovered with Pan-STARRS1 in this work, in Morganson et al. (2012), in Bañados et al. (2014), and in Bañados et al. (2015b). Empty circles represent known quasars discovered by other surveys that satisfy the Pan-STARRS1 selection criteria presented in this paper. Empty squares show known quasars discovered by other surveys that do not comply with the PS1 selection criteria. A representative error bar is shown in the bottom left corner.

our compilation of 1827 L and T dwarfs[19] with the PS1 stacked catalog, taking the closest match within a 2″ radius. There are 986 matches (734 L and 252 T dwarfs) with measurements in the $i_{\rm P1}$, $z_{\rm P1}$, and $y_{\rm P1}$ bands and with a signal-to-noise ratio (S/N) > 5 in the $z_{\rm P1}$ and $y_{\rm P1}$ bands. The PS1 colors of brown dwarfs are represented by small circles in Figure 1.

In this paper we update and extend the *i*-dropout selection ($z \sim 6$ quasars) discussed in detail in Bañados et al. (2014). The *z*-dropout selection ($z \sim 7$ quasars) is discussed in Venemans et al. (2015a), and an update will be given by C. Mazzucchelli et al. (2016, in preparation).

Given the rarity and faintness of these high-redshift quasars plus the numerous foreground objects that can have similar PS1 colors, efficiently finding these quasars poses a big challenge. For that reason, we followed several steps in order to clean up our candidate list. In short, we selected initial high-redshift quasar candidates from the PS1 PV1 or PV2 databases (Section 2.1). This was followed by forced photometry at the position of each candidate in both their stacked and single-epoch images to corroborate the catalog colors and remove artifacts (this process removes about 80% of the initial candidates; see Sections 2.2 and 2.3 in Bañados et al. 2014). We then matched the candidate list to public infrared surveys to

[17] Note that the PS1 magnitudes presented in Bañados et al. (2014, 2015b) and Venemans et al. (2015a) were not corrected for Galactic extinction.

[18] A machine-readable format can be obtained from the online journal. An updated version can be obtained upon request from the authors.

[19] Based on the list compiled by Mace (2014), with additions from Lodieu et al. (2014), Marocco et al. (2015), and Best et al. (2015).

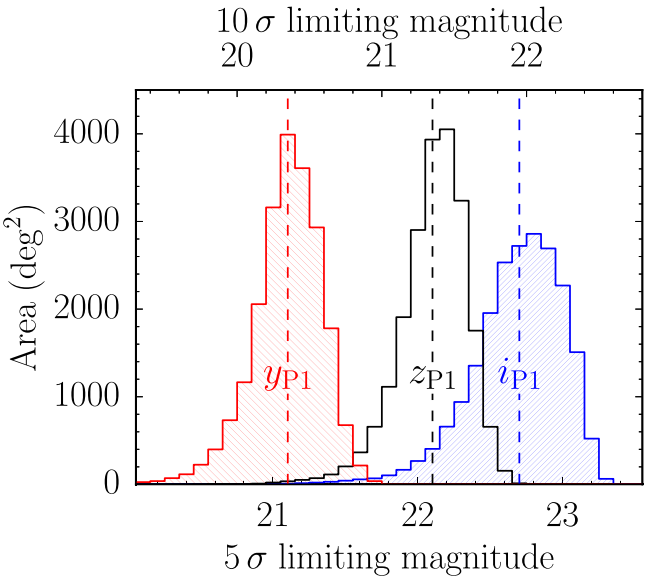

Figure 2. PS1 PV2 5σ extinction-corrected limiting magnitude distributions in our quasar search area for the main bands used in our quasar selection: i_{P1}, z_{P1}, and y_{P1} (see Section 2.1). The vertical dashed lines show the median magnitudes of the survey. For reference the top axis shows the respective 10σ limiting magnitudes.

eliminate or prioritize candidates using the extra information provided by these surveys (Section 2.2). Before following up the candidates, we visually inspected their PS1 stacked and single-epoch images (and their infrared images when available) to ensure that they were real astrophysical objects. We then obtained optical and near-infrared follow-up photometry to remove lower-redshift interlopers (Section 3.1) and then finally acquired the spectra of the remaining candidates (Section 3.2).

2.1. The Pan-STARRS1 Catalog

The selection presented here is based on the PS1 PV1 and PV2 catalogs. Figure 2 shows the PV2 5σ (and 10σ) extinction-corrected i_{P1}, z_{P1}, and y_{P1} limiting magnitude distributions in our search area. The 5σ median limiting magnitudes are (g_{P1}, r_{P1}, i_{P1}, z_{P1}, y_{P1}) = (23.2, 23.0, 22.7, 22.1, 21.1). As in our previous works, we excluded candidates in the Milky Way plane ($|b| < 20°$) and M31 ($7° <$ R.A. $< 14°$; $37° <$ decl. $< 43°$); this yields a survey effective area of 2.05 π steradians. However, this time, we followed up a few bright quasar candidates in the Galactic plane, taking advantage of the Schlegel et al. (1998) dust maps and thus requiring a reddening of $E(B-V) < 0.3$. This resulted in the discovery of two $z \sim 6$ quasars with $|b| < 20°$, a region that had not been explored by other high-redshift quasar surveys (see Section 4.3). While we did not exclude any area around M33 (R.A. $\sim$ 23° and Decl. $\sim$ 30°), candidates in that region were more critically inspected since the number of candidates in that area is larger than that in other regions of the sky.

We also excluded those measurements whose results the Image Processing Pipeline (Magnier 2006, 2007) flagged as suspicious (see Table 6 in Bañados et al. 2014). Furthermore, we required that more than 85% of the expected point-spread function (PSF)-weighted flux in the i_{P1}, z_{P1}, and y_{P1} bands was

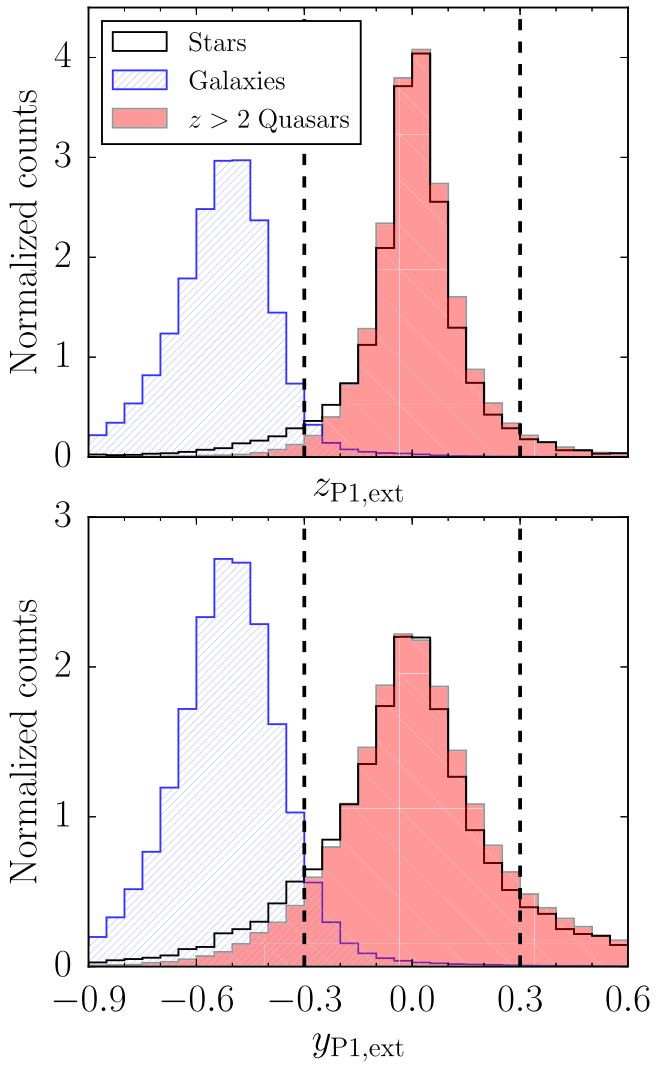

Figure 3. Aperture minus PSF magnitudes ($mag_{P1,ext}$) for the z_{P1} (top) and y_{P1} (bottom) bands for different sources as indicated in the legend. The quasars are taken from the SDSS-DR10 quasar catalog (Pâris et al. 2014), while SDSS spectroscopic stars and galaxies are retrieved from the region 160° < R. A. < 220°; 0° < decl. < 20°. All sources in this figure have S/N(z_{P1}) > 10, S/N(y_{P1}) > 5, $z_{P1} > 19$, and $y_{P1} > 19$. The counts are normalized so that the integrals of the histograms sum to 1 (bin width =0.05). As a part of our quasar candidate selection, we require $(-0.3 < z_{P1,ext} < 0.3)$ *or* $(-0.3 < y_{P1,ext} < 0.3)$ (dashed vertical lines).

located in valid pixels (i.e., that the PS1 catalog entry had PSF_QF > 0.85).

We used the difference between the aperture and PSF magnitudes ($mag_{P1,ext}$) as a proxy to remove extended sources. As a test, we obtained the PS1 information for all $z > 2$ quasars from the SDSS-DR10 quasar catalog (Pâris et al. 2014) and a sample of spectroscopic stars and galaxies from SDSS (DR12; Alam et al. 2015). Figure 3 shows the $z_{P1,ext}$ and $y_{P1,ext}$ histograms for these sources, with the requirement that S/N (z_{P1}) > 10, S/N(y_{P1}) > 5, $z_{P1} > 19$, and $y_{P1} > 19$. The PSF magnitudes for galaxies were systematically fainter than the aperture magnitudes, as expected. Since we were interested in point sources, we required our candidates to satisfy $(-0.3 < z_{P1,ext} < 0.3)$ *or* $(-0.3 < y_{P1,ext} < 0.3)$. With these criteria we excluded 92% of the galaxies while recovering 93% and 97% of the stars and quasars, respectively.

2.1.1. i-Dropout Search ($5.7 \lesssim z \lesssim 6.5$)

In Bañados et al. (2014) we searched for quasars in the upper left region of Figure 1 (i.e., $z_{\rm P1} - y_{\rm P1} < 0.5$ and $i_{\rm P1} - z_{\rm P1} > 2.2$). This is the PS1 color space region where quasars in the redshift range $5.7 \lesssim z \lesssim 6.2$ are best differentiated from brown dwarfs. This is the selection on which we initially focused and therefore the one with the most comprehensive follow-up. In the present work, we extended the search to $z_{\rm P1} - y_{\rm P1} > 0.5$. This allowed us to search for quasars in the redshift range $6.2 \lesssim z \lesssim 6.5$ but admittedly in a region highly contaminated, especially by L and T dwarfs (see the upper right region in Figure 1). Another difference with respect to the selection in Bañados et al. (2014) was that now our initial PS1 color criteria were based on the *dereddened* magnitudes. This allowed us to relax our criteria to $i_{\rm P1} - z_{\rm P1} > 2.0$, but we still prioritized the reddest objects (i.e., $i_{\rm P1} - z_{\rm P1} > 2.2$, horizontal dotted line in Figure 1) for follow-up. Furthermore, in contrast to Bañados et al. (2014), we did not impose any flux restriction (besides the implicit S/N cuts)—i.e., a source could be unrestrictedly bright. The selection criteria can be summarized as follows:

$$((\mathrm{S/N}(i_{\rm P1}) \geqslant 3)\ \mathrm{AND}\ (i_{\rm P1} - z_{\rm P1} > 2.0))\mathrm{OR}\ (i_{\rm P1,lim} - z_{\rm P1} > 2.0) \quad (1a)$$

$$\mathrm{S/N}(g_{\rm P1}) < 3. \quad (1b)$$

Additionally, candidates with $z_{\rm P1} - y_{\rm P1} < 0.5$ were required to comply with the following:

$$\mathrm{S/N}(z_{\rm P1}) > 10 \quad (2a)$$

$$\mathrm{S/N}(y_{\rm P1}) > 5 \quad (2b)$$

$$\mathrm{S/N}(r_{\rm P1}) < 3 \mathrm{OR} (r_{\rm P1} - z_{\rm P1} > 2.2). \quad (2c)$$

The requirements for candidates with $z_{\rm P1} - y_{\rm P1} \geqslant 0.5$ were

$$\mathrm{S/N}(z_{\rm P1}) > 7 \quad (3a)$$

$$\mathrm{S/N}(y_{\rm P1}) > 7 \quad (3b)$$

$$\mathrm{S/N}(r_{\rm P1}) < 3. \quad (3c)$$

2.2. Public Infrared Surveys

We matched our sources with several public infrared surveys to extend and verify the photometry of the quasar candidates. The extra information was used to either remove foreground interlopers or prioritize the subsequent follow-up.

2MASS: The PS1 candidates were matched within 3″ with the Two Micron All Sky Survey (2MASS; Skrutskie et al. 2006). This is a shallow all-sky survey in the *J*, *H*, and *K* bands, with nominal 5σ limiting AB magnitudes of 17.5, 17.3, and 16.9, respectively. Nevertheless, given its large areal coverage, it is ideal to eliminate bright foreground interlopers and even find extremely bright high-redshift quasars (e.g., Wu et al. 2015). In order to remove bright cool dwarfs, we required our candidates to be undetected in 2MASS or to have $y_{\rm P1} - J < 1$ (see Figure 4).

UKIDSS: We matched our objects with the near-infrared data from the UKIDSS survey (Lawrence et al. 2007) using a 2″ matching radius. The UKIDSS Large Area Survey provides *Y*, *J*, *H*, and *K* imaging over ~4000 deg^2, with nominal 5σ AB limiting magnitudes of 21.1, 20.9, 20.2, and 20.3, respectively. We kept the candidates that had $Y - J < 0.8$, $y_{\rm P1} - J < 1$, $y_{\rm P1} - Y < 0.5$, and $Y - J < -(y - J) + 1.2$ (see Figure 4).

VHS: We cross-matched our candidates to the *J*-band catalog of the first data release of the VISTA Hemisphere Survey (VHS; McMahon et al. 2013). This release covers ~8000 deg^2 to a 5σ limiting AB magnitude of $J = 21.1$. We applied the same color criteria as for our 2MASS matched list.

WISE: WISE (Wright et al. 2010) surveyed the entire mid-infrared sky in four bands centered at 3.4, 4.6, 12, and 22 μm (hereafter, *W*1, *W*2, *W*3, and *W*4). In regions that are not confusion limited, the nominal 5σ limiting AB magnitudes of the ALLWISE catalog[20] are $W1 = 19.6$, $W2 = 19.3$, $W3 = 16.7$, and $W4 = 14.6$. Even though more than half of the known $z > 6$ quasars are detected in *WISE*, a selection of high-redshift quasars purely based on *WISE* is extremely difficult owing to their *WISE* colors being hard to distinguish from active galactic nuclei and star-forming galaxies at lower redshifts (Blain et al. 2013). Nevertheless, the combination of *WISE* and optical surveys is a powerful tool to remove or avoid a large fraction of the main foreground contaminants of optical surveys—i.e., cool dwarfs (see Figure 5). We cross-matched our quasar candidates with the ALLWISE catalog within 3″ (but see Appendix B). At this stage, we used the *WISE* information only to prioritize candidates for follow-up observations. Objects with S/N > 3 in *W*1 and *W*2 were assigned a higher priority if their colors fulfilled the additional criteria:

$$-0.2 < W1 - W2 < 0.85$$
$$-0.7 < y_{\rm P1} - W1 < 2.2.$$

For the few objects with S/N > 3 in *W*3, a higher priority was assigned if

$$W2 - W3 > 0.$$

Recently, in part motivated by the quasar selection criteria presented in Carnall et al. (2015), we included an additional prioritization for *i*-dropout candidates:

$$z_{\rm P1} - W2 < 2.5.$$

The dashed lines in Figure 5 show our prioritization criteria. Objects undetected in the ALLWISE catalog or with S/N < 3 in *W*1 or *W*2 were assigned an intermediate priority, while the remaining candidates were given a low priority. Note that we rejected no candidates based on their *WISE* colors and we even discovered quasars that did not fulfill our prioritization criteria.

3. FOLLOW-UP OBSERVATIONS

3.1. Photometry

Since many of our candidates had PS1 magnitudes close to our S/N cuts, we obtained deep optical follow-up imaging to corroborate the PS1 colors and eliminate objects that were scattered into our color selection. Additionally, we obtained deep near-infrared imaging, which provides essential information to efficiently separate cool dwarfs—our main contaminants—from high-redshift quasars (Figure 4). The photometric follow-up observations were carried out over different observing runs and different instruments. We obtained optical and near-infrared images with the MPG 2.2 m/GROND (Greiner et al. 2008), New Technology Telescope (NTT)/EFOSC2 (Buzzoni et al. 1984), NTT/SofI (Moorwood et al. 1998), Calar Alto (CAHA) 3.5 m/Omega2000 (Bizenberger

[20] http://wise2.ipac.caltech.edu/docs/release/allwise

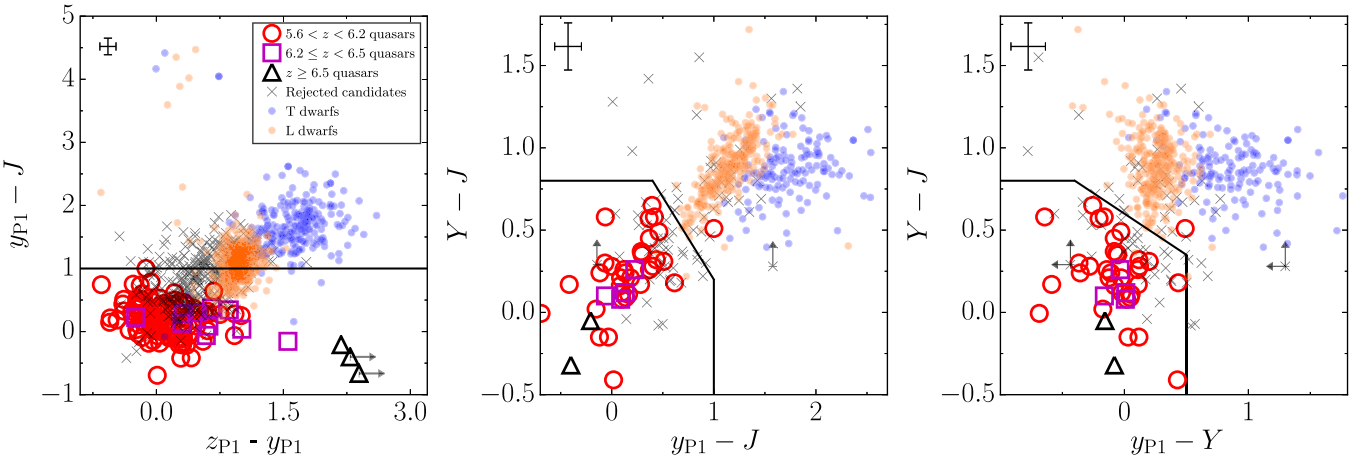

Figure 4. Selection criteria when the Y and/or J bands are available (black solid lines). Empty red circles, magenta squares, and black triangles represent the colors of known quasars at $5.6 < z < 6.2$, $6.2 \leqslant z < 6.5$, and $z \geqslant 6.5$, respectively. L and T dwarfs are shown with small orange and blue circles, respectively. Candidates rejected by follow-up photometry are shown as gray crosses. To enhance the clarity of the figure, the upper limits for brown dwarfs are not displayed. Representative error bars are shown in the upper left corner of each panel. The magnitudes in this figure are not dereddened. Left: $z_{P1} - y_{P1}$ vs. $y_{P1} - J$ color–color diagram. Middle: $y_{P1} - J$ vs. $Y - J$ color–color diagram. Right: $y_{P1} - Y$ vs. $Y - J$ color–color diagram.

et al. 1998; Bailer-Jones et al. 2000), CAHA 2.2 m/CAFOS[21], MMT/SWIRC (Brown et al. 2008), and du Pont/Retrocam[22]; see Table 1 for details of the observations and filters used.

We reduced the data and obtained the zero points following standard procedures (e.g., see Section 2.6 in Bañados et al. 2014). The near-infrared data taken with the 2.5 m du Pont telescope were reduced by collaborators from the Carnegie Supernova Project, with dark subtraction, flat fielding, and bad-pixel masked final combination as detailed in Hamuy et al. (2006). For completeness, we provide below the color conversions used to calibrate our follow-up imaging:

$$
\begin{aligned}
g_{\rm G} &= g_{\rm P1} + 0.332 \times (g_{\rm P1} - r_{\rm P1}) + 0.055 \\
r_{\rm G} &= r_{\rm P1} + 0.044 \times (r_{\rm P1} - i_{\rm P1}) - 0.001 \\
i_{\rm G} &= i_{\rm P1} - 0.089 \times (r_{\rm P1} - i_{\rm P1}) + 0.001 \\
z_{\rm G} &= z_{\rm P1} - 0.214 \times (z_{\rm P1} - y_{\rm P1}) \\
J_{\rm G} &= J_{\rm 2M} - 0.012 \times (J_{\rm 2M} - H_{\rm 2M}) + 0.004 \\
H_{\rm G} &= H_{\rm 2M} + 0.030 \times (H_{\rm 2M} - K_{\rm 2M}) + 0.009 \\
I_{\rm E} &= i_{\rm P1} - 0.149 \times (i_{\rm P1} - z_{\rm P1}) - 0.001 \\
Z_{\rm E} &= z_{\rm P1} - 0.265 \times (z_{\rm P1} - y_{\rm P1}) \\
z_{\rm O2K} &= z_{\rm P1} - 0.245 \times (z_{\rm P1} - y_{\rm P1}) \\
Y_{\rm O2K} &= y_{\rm P1} - 0.413 \times (z_{\rm P1} - y_{\rm P1}) + 0.012 \\
J_{\rm O2K} &= J_{\rm 2M} + 0.093 \times (J_{\rm 2M} - H_{\rm 2M}) \\
i_{\rm C} &= i_{\rm P1} - 0.098 \times (i_{\rm P1} - z_{\rm P1})
\end{aligned}
$$

where $J_{\rm 2M}$, $H_{\rm 2M}$, and $K_{\rm 2M}$ are the 2MASS magnitudes in the AB system. $J_{\rm S}$, $J_{\rm SWIRC}$, $J_{\rm R}$, and $H_{\rm O2K}$ are calibrated against 2MASS.

Candidates were considered foreground interlopers if they had $Y - J > 0.8$, $y_{\rm P1} - J > 1$, $y_{\rm P1} - Y > 0.5$, or $Y - J > -(y - J) + 1.2$ (see Section 2.2 and Figure 4).

The NTT/EFOSC2 filters $I_{\rm E}$ (#705) and $Z_{\rm E}$ (#623) are significantly different from the $i_{\rm P1}$ and $z_{\rm P1}$ filters. For candidates observed with $I_{\rm E}$, $Z_{\rm E}$, and/or J bands, we used the color–color diagrams in Figure 6 to select targets for spectroscopic follow-up.

[21] www.caha.es/CAHA/Instruments/CAFOS/index.html
[22] www.lco.cl/telescopes-information/irenee-du-pont/instruments/website/retrocam

Candidates rejected for not meeting at least one of our photometric follow-up criteria are shown as crosses in Figures 4–6. Tables 2 and 3 present the imaging follow-up of the PS1-discovered quasars selected with the criteria of Sections 2.1.1 with $z_{\rm P1} - y_{\rm P1} < 0.5$ and $z_{\rm P1} - y_{\rm P1} \geqslant 0.5$, respectively. Table 4 lists the imaging follow-up of three PS1-discovered quasars that were selected using more relaxed selection criteria in terms of their optical colors and two that were found at low Galactic latitudes ($|b| < 20°$). These five objects are discussed further in Section 4.3.

3.2. Spectroscopy

We spectroscopically followed up candidates that satisfied the selection from the previous sections. This spectroscopic campaign was carried out using several instruments at different telescopes: EFOSC2 at the NTT telescope in La Silla, the Focal Reducer / Low-Dispersion Spectrograph 2 (FORS2; Appenzeller & Rupprecht 1992) at the Very Large Telescope (VLT), the Folded-Port Infrared Echellette (FIRE; Simcoe et al. 2008, 2013) spectrometer and the Low-Dispersion Survey Spectrograph (LDSS3) at the Baade and Clay Telescopes at Las Campanas Observatory, the Low-Resolution Imaging Spectrometer (LRIS; Oke et al. 1995) at the Keck I 10 m Telescope on Mauna Kea, the Double Spectrograph (DBSP; Oke & Gunn 1982) on the 200 inch (5 m) Hale Telescope at Palomar Observatory (P200), the Red-Channel Spectrograph (Schmidt et al. 1989) on the 6.5 m MMT Telescope, the Cassegrain TWIN Spectrograph at the 3.5 m Calar Alto Telescope (CAHA 3.5 m), and the Multi-object Double Spectrograph (MODS; Pogge et al. 2010) and LUCI spectrograph (Seifert et al. 2003) at the Large Binocular Telescope (LBT).

The details of the spectroscopic observations of the PS1-discovered quasars are shown in Table 5. There were 11 candidates for which the spectroscopy revealed a non-quasar interloper; their photometric information is presented in Appendix C. The spectra were reduced using standard routines including bias subtraction, flat fielding, sky subtraction, and wavelength calibration using exposures of He, HgCd, and Ne arc lamps.

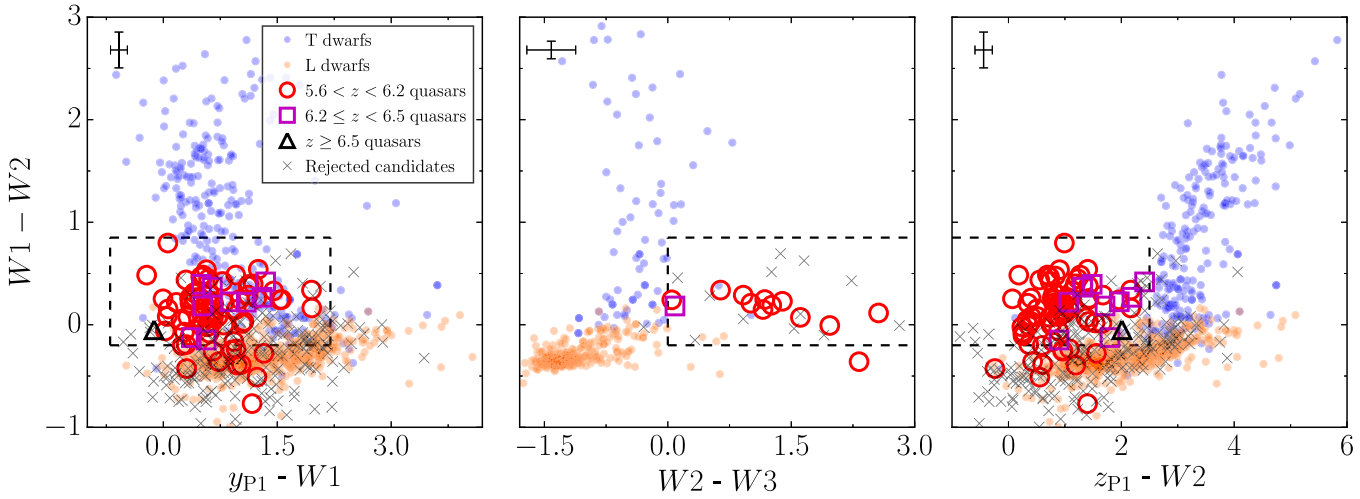

Figure 5. Prioritization criteria for candidates detected in *WISE* with S/N > 3 (black dashed lines). Empty red circles, magenta squares, and black triangles represent the colors of known quasars at $5.6 < z < 6.2$, $6.2 \leqslant z < 6.5$, and $z \geqslant 6.5$, respectively. L and T dwarfs are shown with small orange and blue circles, respectively. Candidates rejected by follow-up photometry are shown as gray crosses. To enhance the clarity of the figure, the upper limits for brown dwarfs are not displayed. Representative error bars are shown in the upper left corner of each panel. The magnitudes in this figure are not dereddened. Left: $y_{\rm P1} - W1$ vs. $W1 - W2$ color–color diagram. Middle: $W2 - W3$ vs. $W1 - W2$ color–color diagram. Right: $z_{\rm P1} - W2$ vs. $W1 - W2$ color–color diagram. These criteria are not used for z-dropout candidates (cf., Venemans et al. 2015a).

4. 77 NEW QUASARS AT $z > 5.6$

We discovered 77 quasars at $5.6 < z < 6.7$ while mining the PS1 database; out of these, 63 are new discoveries presented in this paper. In Morganson et al. (2012) and Bañados et al. (2014, 2015b) we presented our first 11 i-dropout ($z \sim 6$) quasars, while our first 3 z-dropout ($z > 6.5$) quasars were introduced in Venemans et al. (2015a). For completeness we include these quasars in the tables and figures of this section. The spectra of all PS1 quasars discovered to date are shown in Figure 7. The i-dropout spectra are scaled to match their dereddened $z_{\rm P1}$ magnitude, while the z-dropouts are scaled to their near-infrared magnitudes (see Venemans et al. 2015a).

The names, redshifts, and coordinates of these newly discovered quasars are listed in Table 7, and their dereddened PS1 PV3 magnitudes and corresponding $E(B - V)$ values are given in Table 8.

4.1. Redshifts

Estimating accurate quasar systemic redshifts from broad emission lines is challenging. At $z > 5.6$, it is especially difficult as the most prominent emission lines in optical spectra are Lyα, which is highly affected by absorption at these redshifts, and high-ionization lines, such as C IV and Si IV +O IV], which are known to be poor estimators of systemic redshifts (Richards et al. 2002; De Rosa et al. 2014; Shen et al. 2016). Ideally, we would prefer to measure the redshifts from atomic or molecular emission lines, such as [C II] and CO, which provide host galaxy redshifts as accurate as $\Delta z < 0.002$ (e.g., Wang et al. 2010; Bañados et al. 2015a). Alternatively, for quasars at $6.0 \lesssim z \lesssim 7.4$, the low-ionization line Mg II can be observed in the near-infrared K-band. This line is thought to be a more accurate tracer of the systemic redshift compared to high-ionization lines, although at $z \sim 6$ significant shifts of 480 ± 630 km s^{-1} are found between the redshift of the Mg II line and that of atomic or molecular lines (see discussion in Venemans et al. 2016). In this paper, we report redshifts estimated from fittings to the [C II], CO, or Mg II lines when available.

However, for the vast majority of the quasars presented here, only optical spectra are available, several of which show only weak emission lines. We estimated the redshifts for these quasars following a template fitting approach. We performed a χ^2 minimization relative to two quasar templates. One is the composite $z \sim 6$ SDSS quasar spectra from Fan et al. (2006), and the other is the template from Selsing et al. (2016). The latter was chosen over other typical quasar templates because it was created only from bright quasars, which have comparable luminosities to the $z \sim 6$ quasars discovered in this work. The redshifts derived from these two templates generally agreed well, but sometimes differences of up to 0.05 were observed. In these cases, the fits were visually inspected to assess which one was the best match. Conservatively, for these cases we report redshifts with significance up to the second decimal only.

4.2. Rest-frame 1450 Å Magnitudes

Another important quantity is the magnitude at rest-frame 1450 Å (m_{1450}), which plays a key role in the estimation of the quasar luminosity function. At $z > 5.6$ the rest-frame 1450 Å is shifted to observed wavelengths >9570 Å. Thus, m_{1450} is hard to estimate for $z > 5.6$ quasars, especially when only optical spectra are available.

The main challenge is to determine the continuum, which is mostly prevented by the low rest-frame wavelength coverage of optical spectra ($\lambda_{\rm rest} < 1500$ Å) and often also by low S/N. In the literature, several methods are used to estimate these quantities, including interpolation and fitting a power law of the form $f_\nu = C \times \nu^{\alpha_\nu}$ to regions of the continuum that are generally uncontaminated by emission lines. In the latter case, a good fit of the continuum is typically not possible unless the power law index α_ν is fixed. A range of α_ν indices are used by different authors, the most common being $\alpha_\nu = -0.5$, which is consistent with the average quasar UV continuum slope found by Vanden Berk et al. (2001). Recently, Selsing et al. (2016) found that $\alpha_\nu = -0.3$ is a good fit for luminous quasars without significant host contamination, as is expected for our luminous $z > 5.6$ quasars. Furthermore, some of the m_{1450}

Table 1
Imaging Observations of Quasar Candidates

Date	Telescope/Instrument	Filters	Exposure Time
2012 May 21–24	MPG 2.2 m/GROND	g_G, r_G, i_G, z_G, J_G, H_G, K_G	460–1440 s
2013 Jan 14–18	MPG 2.2 m/GROND	g_G, r_G, i_G, z_G, J_G, H_G, K_G	460–1440 s
2013 Jan 26	CAHA 3.5 m/Omega2000	z_{O2K}, Y_{O2K}, J_{O2K}	900 s
2013 Mar 13–16	NTT/EFOSC2	I_E, Z_E	300 s
2013 Mar 23–29	CAHA 3.5 m/Omega2000	z_{O2K}, Y_{O2K}, J_{O2K}	300 s
2013 Apr 16–18	CAHA 2.2 m/CAFOS	i_C	1000s
2013 Apr 26–27	CAHA 3.5 m/Omega2000	z_{O2K}, Y_{O2K}, J_{O2K}	300–600 s
2013 Aug 18–19	CAHA 3.5 m/Omega2000	z_{O2K}, Y_{O2K}, J_{O2K}	300–600 s
2013 Sep 7–10	MPG 2.2 m/GROND	g_G, r_G, i_G, z_G, J_G, H_G, K_G	460–1440 s
2013 Sep 27–Oct 1	NTT/EFOSC2	I_E, Z_E	600 s
2013 Oct 16–21	CAHA 3.5 m/Omega2000	z_{O2K}, Y_{O2K}, J_{O2K}, H_{O2K}	300 s
2013 Nov 9–12	CAHA 2.2 m/CAFOS	i_C	1250s
2013 Nov 15–17	CAHA 3.5 m/Omega2000	z_{O2K}, Y_{O2K}, J_{O2K}	300 s
2013 Dec 14–15	CAHA 2.2 m/CAFOS	i_C	1500 s
2014 Jan 24–Feb 5	MPG 2.2 m/GROND	g_G, r_G, i_G, z_G, J_G, H_G, K_G	460–1440 s
2014 Mar 2–6	NTT/EFOSC2	I_E, Z_E	600 s
2014 Mar 2 and 5	NTT/SofI	J_S	300 s
2014 Mar 16–19	CAHA 3.5 m/Omega2000	z_{O2K}, Y_{O2K}, J_{O2K}	300 s
2014 Apr 22–24	CAHA 2.2 m/CAFOS	i_C	2400 s
2014 May 9	CAHA 3.5 m/Omega2000	z_{O2K}, Y_{O2K}, J_{O2K}	300 s
2014 Jul 23–27	NTT/EFOSC2	I_E, Z_E	600 s
2014 Jul 25	NTT/SofI	J_S	600 s
2014 Aug 7 and 11–13	CAHA 3.5 m/Omega2000	Y_{O2K}, J_{O2K}	600 s
2014 Aug 22–24	CAHA 2.2 m/CAFOS	i_C	1800 s
2014 Sep 12 and 14	CAHA 3.5 m/Omega2000	Y_{O2K}, J_{O2K}	600 s
2014 Sep 16–17	CAHA 2.2 m/CAFOS	i_C	1800 s
2014 Sep 17–25	MPG 2.2 m/GROND	g_G, r_G, i_G, z_G, J_G, H_G, K_G	460–1440s
2014 Dec 13–21	MPG 2.2 m/GROND	g_G, r_G, i_G, z_G, J_G, H_G, K_G	460–1440s
2015 Feb 7 and 28	CAHA 3.5 m/Omega2000	z_{O2K}, Y_{O2K}, J_{O2K}	600–900 s
2015 Feb 19–23	NTT/EFOSC2	I_E, Z_E	600 s
2015 Feb 22	NTT/SofI	J_S	300 s
2015 Mar 1 and 11–12	CAHA 3.5 m/Omega2000	z_{O2K}, Y_{O2K}, J_{O2K}, H_{O2K}	600–900 s
2015 Apr 13–15	CAHA 2.2 m/CAFOS	i_C	1800s
2015 May 18–28	MPG 2.2 m/GROND	g_G, r_G, i_G, z_G, J_G, H_G, K_G	460–1440 s
2015 Jun 8	MMT/SWIRC	J_{SWIRC}	300 s
2015 Jul 21–23	NTT/EFOSC2	I_E, Z_E	600 s
2015 Jul 20 and 23	NTT/SofI	J_S	300 s
2015 Aug 7–13	MPG 2.2 m/GROND	g_G, r_G, i_G, z_G, J_G, H_G, K_G	460–1440 s
2015 Sep 15–20	CAHA 2.2 m/CAFOS	i_C	1800 s
2015 Sep 28–Oct 1	CAHA 3.5 m/Omega2000	z_{O2K}, J_{O2K}	300–600 s
2015 Nov 4–8	MPG 2.2 m/GROND	g_G, r_G, i_G, z_G, J_G, H_G, K_G	460–1440 s
2016 Jan 12	CAHA 2.2 m/CAFOS	i_C	3360 s
2016 Jan 30–Feb 1–2	NTT/SofI	J_S	300 s
2016 Jan 31–Feb 2–3	NTT/EFOSC2	I_E, Z_E	300–900 s
2016 Mar 30–31	du Pont/RetroCam	Y_R, J_R	220–1200 s

values cited in the literature were estimated with outdated redshifts; much more accurate values are currently available. This fact and the fact that the literature values for m_{1450} are not calculated in a consistent manner could eventually have repercussions on other fundamental measurements, such as those of the quasar luminosity function.

In order to determine m_{1450} in a consistent way and circumvent the fact that most of our spectra have a limited wavelength coverage and some of them have poor S/N, we adopted the following approach. We assumed a power law continuum slope $\alpha_\nu = -0.3$ (Selsing et al. 2016). For quasars in the redshift range $5.6 < z < 6.3$ we calculated m_{1450} by extrapolating the y_{P1} magnitude ($\lambda_{eff} = 9627.7$ Å). In this redshift range, the extrapolation to rest-frame 1450 Å is of the order of ∼100 Å or less. In some cases the y_{P1} band will be contaminated by the Si IV+O IV] emission line, which has a typical (rest-frame) equivalent width of 8 Å (Vanden Berk et al. 2001). Given the width of the y_{P1} band of ∼800 Å (Tonry et al. 2012), Si IV+O IV] would contribute less than ∼10% of the flux in the broad band. At $z \geqslant 6.3$ contributions from Lyα and N V might start being significant for the flux measured in y_{P1}. Therefore, at these redshifts we extrapolated m_{1450} from their J-band magnitude ($\lambda_{eff} = 12444.0$ Å). The J band is in a region clean of strong emission lines up to $z \sim 7$; this region is contaminated by C IV, which has a typical (rest-frame) equivalent width of ∼24 Å. Even though C IV is brighter than

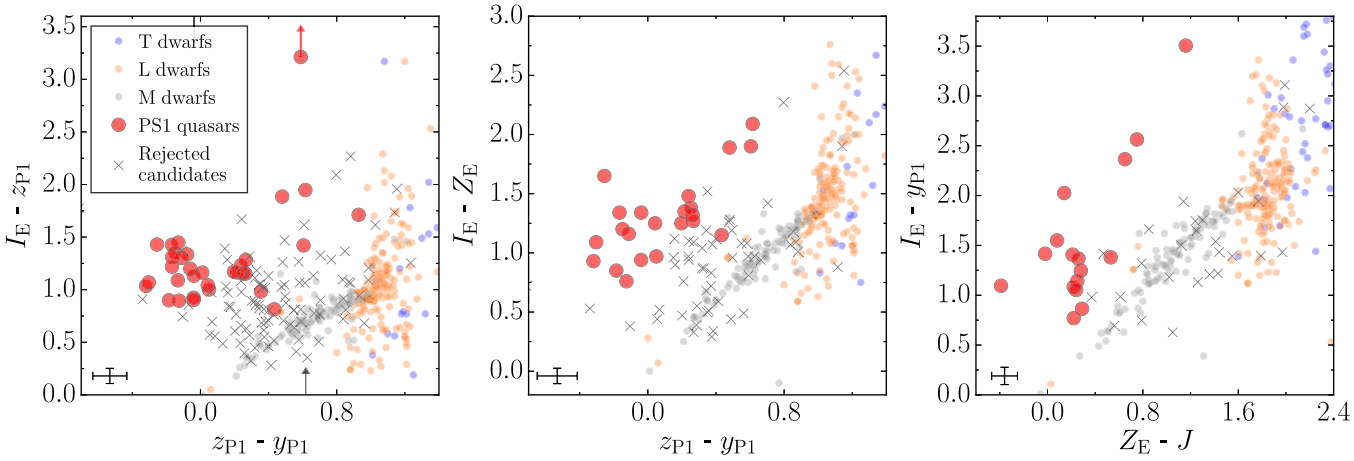

Figure 6. Diagrams used to select candidates for follow-up spectroscopy based on their NTT imaging follow-up. The brown dwarf colors in this figure are synthetic colors obtained from spectra taken from the SpeX Prism Spectral Libraries (http://pono.ucsd.edu/~adam/browndwarfs/spexprism/). Candidates rejected by follow-up photometry are shown as gray crosses. Representative error bars are shown in the lower left corner of each panel. The magnitudes in this figure are not dereddened. Left: $z_{P1} - y_{P1}$ vs. $I_E - z_{P1}$ color–color diagram. Middle: $z_{P1} - y_{P1}$ vs. $I_E - Z_E$ color–color diagram. Right: $Z_E - J$ vs. $I_E - y_{P1}$ color–color diagram.

Si IV+O IV], the J band is also wider than the y_{P1} band (~1500 Å), and thus, the contamination should be of comparable order. The extrapolations from the J-band magnitude to m_{1450} are of the order of 100–300 Å. We also computed the rest-frame magnitude assuming a slope of $\alpha_\nu = -0.5$ and found that the absolute differences are negligible (mean: 0.02; standard deviation: 0.02; median: 0.01). This is due to the effective wavelengths of our chosen filters, which minimize the extrapolation.

We followed this approach for all published $z > 5.6$ quasars with information in the y_{P1} or J bands. For comparison, the m_{1450} literature values compiled by Calura et al. (2014) differ from ours by -0.03 ± 0.31 mag. The observed and absolute magnitudes at rest-frame 1450 Å are listed in Table 7.

4.3. Notes on Selected Objects

In this section we discuss some of the new quasars, including five PS1 quasars that were not selected using the criteria of Section 2. The objects are sorted by R.A.

4.3.1. PSO J000.3401+26.8358 ($z = 5.75$)

This quasar has a color $i_{P1} - z_{P1} = 1.97$ and is therefore just below our selection criteria presented in Section 2. However, it was targeted for follow-up because it was relatively bright ($z_{P1} = 19.28$) and it did satisfy all the other criteria, including good *WISE* and $y_{P1} - J$ colors (see Section 2.2 and Figures 5 and 4).

4.3.2. PSO J055.4244–00.8035 ($z = 5.68$)

This quasar was discovered according to the selection criteria presented in Bañados et al. (2015b). That selection was based on the PS1 PV1 catalog and further required a radio-counterpart in the Faint Images of the Radio Sky at Twenty cm survey (FIRST; Becker et al. 1995), which allowed us to relax the requirements on optical colors. This is among the radio-loudest quasars known at $z > 5.5$ (see Figure 2 in Bañados et al. 2015b). While the PV1 $i_{P1} - z_{P1}$ color for this quasar is a lower limit of $i_{P1} - z_{P1} > 1.3$, its PV3 $i_{P1} - z_{P1}$ color is a detection of $i_{P1} - z_{P1} = 2.08$. Therefore, with the deeper PV3 i_{P1} band this quasar does satisfy the selection criteria of Section 2.

4.3.3. PSO J089.9394–15.5833 ($z = 6.05$)

This quasar is located at a Galactic latitude of $b = -18.^\circ31$, in a region with $E(B - V) = 0.30$. This is the first $z > 5.6$ quasar discovered within $|b| < 20^\circ$ of the Milky Way plane. In addition, with $y_{P1} - J = 1.0$ and $Y - J = 0.51$ it does not satisfy the criteria of Figure 4, although its Y-band follow-up was taken after the discovery of this quasar (see Tables 1 and 4).

4.3.4. PSO J108.4429+08.9257 ($z = 5.92$)

Similar to P089–15, this quasar is located within the Galactic plane with $b = 8.^\circ99$ and $E(B - V) = 0.09$. Unlike P089–15 though, P108+08 satisfies our color selection. The discovery of both P089–15 and P108+08 opens up a new area for quasar searches: regions closer to the Milky Way plane but with low extinction values ($E(B - V) < 0.3$).

4.3.5. PSO J135.3860+16.2518 ($z = 5.63$)

Similar to P055–00, this quasar was selected according to the PS1/FIRST criteria presented in Bañados et al. (2015b). P135+16 is also among the radio-loudest quasars at $z > 5.5$ (see also Appendix B). Its PV1 and PV3 $i_{P1} - z_{P1}$ colors do not differ much: $i_{P1} - z_{P1} = 1.70$ versus $i_{P1} - z_{P1} = 1.78$. This color is too blue for the color cuts typically applied in optical searches for high-redshift quasars (for instance, the color cuts presented in this work). Thus, this quasar would have been missed if not for its strong radio emission.

4.3.6. PSO J245.0636–00.1978 ($z = 5.68$)

This quasar was selected from the PV2 database with S/N (y_{P1}) = 5, i.e., just within the limit of our selection criteria (see Equation (2b)). However, the PV3 y_{P1} band of this object has S/N(y_{P1}) = 4.5, and we would have therefore missed this quasar even though it satisfies every other criterion.

4.3.7. PSO J210.8296+09.0475 ($z = 5.88$)

This quasar was independently discovered by Jiang et al. (2015), who reported a slightly lower redshift ($z = 5.86$), but one consistent within the uncertainties.

Table 2
Follow-up Photometry of the PS1-discovered Quasars Selected as *i*-dropouts with $i_{P1} - z_{P1} < 0.5$ ($5.7 \lesssim z \lesssim 6.2$)

Quasar	z	Photometry (mag)
P002–06	5.93	$i_G > 23.01$ $z_G = 20.55 \pm 0.05$ $J_G = 19.86 \pm 0.14$ $H_G = 19.92 \pm 0.20$ $I_E = 21.72 \pm 0.09$
P002+32	6.10	$i_C > 23.30$ $z_{O2K} = 21.65 \pm 0.09$ $J_{O2K} = 21.38 \pm 0.19$
P004+17	5.80	$i_C = 23.34 \pm 0.35$ $z_{O2K} = 21.14 \pm 0.14$ $Y_{O2K} = 20.79 \pm 0.22$ $J_{O2K} = 20.67 \pm 0.16$
P004–24	5.68	$i_G = 22.09 \pm 0.15$ $z_G = 19.66 \pm 0.03$ $J_G = 19.30 \pm 0.08$ $H_G = 18.97 \pm 0.08$ $I_E = 20.81 \pm 0.03$ $Z_E = 19.56 \pm 0.04$
P007+04	6.00	$i_G = 22.74 \pm 0.24$ $z_G = 20.39 \pm 0.04$ $J_G = 19.77 \pm 0.11$ $H_G = 19.71 \pm 0.15$
P009–08	5.72	$i_G = 22.24 \pm 0.10$ $z_G = 20.23 \pm 0.02$ $J_G = 19.79 \pm 0.08$ $H_G = 19.70 \pm 0.13$
P021–25	5.79	$i_G = 22.83 \pm 0.17$ $z_G = 19.84 \pm 0.01$ $J_G = 19.21 \pm 0.05$ $H_G = 19.40 \pm 0.08$
P023–02	5.90	$i_G = 23.32 \pm 0.20$ $z_G = 20.38 \pm 0.02$ $J_G = 19.78 \pm 0.10$ $H_G = 19.44 \pm 0.11$ $I_E = 21.57 \pm 0.05$
P025–11	5.85	$i_G = 22.49 \pm 0.11$ $z_G = 20.25 \pm 0.03$ $J_G = 19.65 \pm 0.06$ $H_G = 19.37 \pm 0.07$
P029–29	5.99	$i_G = 21.84 \pm 0.06$ $z_G = 19.44 \pm 0.02$ $J_G = 19.07 \pm 0.04$ $H_G = 19.09 \pm 0.05$ $I_E = 20.54 \pm 0.01$ $Z_E = 19.29 \pm 0.02$
P037–28	6.00	$i_G = 23.19 \pm 0.15$ $z_G = 20.78 \pm 0.04$ $J_G = 20.41 \pm 0.14$ $H_G = 20.59 \pm 0.26$
P040+17	5.68	$i_C = 22.43 \pm 0.39$ $z_{O2K} = 20.83 \pm 0.06$ $J_{O2K} = 20.43 \pm 0.10$
P042–02	5.89	$i_G = 23.20 \pm 0.20$ $z_G = 20.63 \pm 0.03$ $J_G = 20.41 \pm 0.10$ $H_G = 20.42 \pm 0.14$ $I_E = 21.53 \pm 0.04$
P045–22	5.68	$i_G = 22.78 \pm 0.10$ $z_G = 20.35 \pm 0.03$ $J_G = 19.65 \pm 0.08$ $H_G = 19.42 \pm 0.08$
P049–26	5.94	$I_E = 22.14 \pm 0.05$ $J_S = 20.94 \pm 0.05$
P053–15	5.87	$I_E = 21.77 \pm 0.02$ $Z_E = 20.61 \pm 0.06$
P055–00	5.68	$i_G = 22.16 \pm 0.18$ $z_G = 20.58 \pm 0.05$ $J_G = 20.08 \pm 0.16$ $H_G = 20.03 \pm 0.22$
P056–16	5.99	$I_E = 21.20 \pm 0.03$ $Z_E = 19.86 \pm 0.07$ $J_{O2K} = 20.25 \pm 0.10$ $H_{O2K} = 19.72 \pm 0.09$
P060+24	6.18	$i_G > 23.44$ $z_G = 20.48 \pm 0.03$ $J_G = 19.68 \pm 0.09$ $H_G = 19.68 \pm 0.15$ $i_C = 22.96 \pm 0.29$ $z_{O2K} = 20.40 \pm 0.05$ $Y_{O2K} = 19.75 \pm 0.40$ $J_{O2K} = 19.71 \pm 0.05$
P065–19	6.12	$i_G > 23.30$ $z_G = 19.93 \pm 0.03$ $J_G = 19.90 \pm 0.15$ $H_G = 19.34 \pm 0.15$
P071–04	5.89	$i_G = 22.08 \pm 0.09$ $z_G = 20.34 \pm 0.02$ $J_G = 20.27 \pm 0.07$ $H_G = 20.4 \pm 0.13$
P071–02	5.69	$I_E = 20.23 \pm 0.02$ $Z_E = 19.26 \pm 0.02$ $J_{O2K} = 19.02 \pm 0.03$ $H_{O2K} = 19.00 \pm 0.03$
P075–07	5.88	$I_E = 21.87 \pm 0.06$ $Z_E = 20.60 \pm 0.03$ $J_{O2K} = 20.52 \pm 0.12$ $H_{O2K} = 20.45 \pm 0.21$
P127+03	5.85	$i_G > 23.27$ $z_G = 20.98 \pm 0.06$ $J_G = 20.80 \pm 0.21$ $H_G = 20.43 \pm 0.29$
P135–13	5.91	$i_G = 23.34 \pm 0.21$ $z_G = 20.50 \pm 0.02$ $J_G = 20.80 \pm 0.14$ $H_G = 20.52 \pm 0.20$
P157–02	5.88	$I_E = 21.22 \pm 0.03$ $J_S = 20.20 \pm 0.10$ $Y_R = 20.29 \pm 0.05$
P167+56	5.95	$i_C = 23.40 \pm 0.24$ $z_{O2K} = 20.91 \pm 0.04$ $J_{O2K} = 20.31 \pm 0.14$
P172+26	5.77	$i_C = 22.89 \pm 0.14$ $z_{O2K} = 20.84 \pm 0.09$ $J_{O2K} = 20.44 \pm 0.14$
P174–12	5.81	$I_E = 21.30 \pm 0.07$ $z_{O2K} = 19.93 \pm 0.11$ $J_{O2K} = 20.66 \pm 0.30$
P175–20	5.69	$I_E = 21.55 \pm 0.03$ $Z_E = 20.21 \pm 0.03$
P178–12	5.83	$I_E = 22.08 \pm 0.02$ $Z_E = 20.76 \pm 0.06$ $Y_R = 21.02 \pm 0.09$ $J_R = 20.78 \pm 0.09$
P183–12	5.86	$I_E = 20.69 \pm 0.03$ $Z_E = 19.31 \pm 0.02$
P184+01	6.20	$I_E = 22.66 \pm 0.06$ $Z_E = 21.01 \pm 0.03$
P187–02	5.77	$i_G = 23.08 \pm 0.24$ $z_G = 21.18 \pm 0.06$ $J_G = 20.73 \pm 0.13$ $H_G = 20.48 \pm 0.21$
P187+04	5.89	$I_E = 21.85 \pm 0.04$ $Z_E = 21.00 \pm 0.04$
P194+25	5.91	$I_E = 21.69 \pm 0.04$ $Z_E = 20.60 \pm 0.08$
P197+25	5.84	$I_E = 22.2 \pm 0.07$ $Z_E = 20.72 \pm 0.10$ $i_C = 23.51 \pm 0.23$
P201+57	5.74	$z_{O2K} = 20.84 \pm 0.06$ $J_{O2K} = 20.16 \pm 0.24$
P209–26	5.72	$i_G = 21.86 \pm 0.07$ $z_G = 19.56 \pm 0.01$ $J_G = 19.35 \pm 0.05$ $H_G = 19.11 \pm 0.06$ $I_E = 20.33 \pm 0.01$ $Z_E = 19.57 \pm 0.01$
P210+40	6.04	$i_C > 23.25$
P210+09	5.88	$I_E = 21.51 \pm 0.05$ $z_{O2K} = 20.66 \pm 0.05$ $J_{O2K} = 21.03 \pm 0.23$
P210–12	5.84	$i_G > 21.99$ $z_G > 21.07$ $J_G > 20.13$ $H_G > 19.72$ $I_E = 22.35 \pm 0.06$ $Z_E = 21.00 \pm 0.03$
P212–15	5.83	$i_G > 23.51$ $z_G = 21.63 \pm 0.08$ $J_G = 20.63 \pm 0.15$
P213–22	5.92	$I_E = 20.70 \pm 0.02$ $Z_E = 19.77 \pm 0.01$
P213–13	5.78	$I_E = 22.05 \pm 0.06$
P215–16	5.73	$i_G = 21.72 \pm 0.17$ $z_G = 19.66 \pm 0.05$ $J_G = 19.06 \pm 0.08$ $H_G = 19.34 \pm 0.14$

Table 2
(Continued)

Quasar	z	Photometry (mag)
		$I_E = 20.09 \pm 0.02$ $Z_E = 19.15 \pm 0.02$
		$i_C = 22.29 \pm 0.10$
P228+21	5.92	$i_C > 23.99$ $z_{O2K} = 21.12 \pm 0.13$ $J_{O2K} = 20.89 \pm 0.18$
P235+17	5.82	$z_{O2K} = 19.28 \pm 0.16$ $J_{O2K} = 19.92 \pm 0.08$
P236+16	5.82	$I_E = 22.18 \pm 0.07$
		$i_C = 22.42 \pm 0.14$ $z_{O2K} = 20.87 \pm 0.10$ $J_{O2K} = 20.73 \pm 0.12$
P238–06	5.81	$i_G > 23.23$ $z_G = 20.65 \pm 0.05$ $J_G = 20.11 \pm 0.12$
P239–07	6.11	$I_E = 21.89 \pm 0.05$ $Z_E = 20.00 \pm 0.03$
P242–12	5.83	$i_G = 22.64 \pm 0.17$ $z_G = 20.10 \pm 0.02$ $J_G = 19.59 \pm 0.08$ $H_G = 19.66 \pm 0.15$
P267+22	5.95	$i_C = 23.32 \pm 0.17$ $z_{O2K} = 21.14 \pm 0.15$ $J_{O2K} = 21.02 \pm 0.22$
P293+71	6.08	$i_C > 23.53$ $z_{O2K} = 20.36 \pm 0.11$ $Y_{O2K} = 20.32 \pm 0.19$ $J_{O2K} = 19.67 \pm 0.05$
P308–27	5.80	$i_G = 21.97 \pm 0.09$ $z_G = 19.82 \pm 0.02$ $J_G = 19.46 \pm 0.06$ $H_G = 19.62 \pm 0.09$
P319–10	5.90	$i_G = 22.55 \pm 0.09$ $z_G = 20.27 \pm 0.02$ $J_G = 20.02 \pm 0.05$ $H_G = 19.79 \pm 0.08$
		$I_E = 21.21 \pm 0.03$
P320–24	5.73	$i_G = 22.84 \pm 0.21$ $z_G = 20.59 \pm 0.04$ $J_G = 20.26 \pm 0.10$ $H_G = 19.34 \pm 0.07$
P328–09	5.92	$I_E = 21.69 \pm 0.04$ $Z_E = 20.54 \pm 0.04$
P340–18	6.01	$i_G = 23.32 \pm 0.17$ $z_G = 20.11 \pm 0.04$ $J_G = 20.28 \pm 0.08$ $H_G = 19.90 \pm 0.11$
P357+06	5.81	$i_G > 23.63$ $z_G = 21.91 \pm 0.11$ $J_G = 21.69 \pm 0.35$
P359–06	6.15	$i_G > 22.99$ $z_G = 20.14 \pm 0.04$ $J_G = 19.85 \pm 0.10$ $H_G = 19.47 \pm 0.13$

Note. Quasars sorted by right ascension. Their complete names and coordinates are given in Table 7. Their PS1 magnitudes are listed in Table 8.

(This table is available in its entirety in machine-readable form.)

Table 3
Follow-up Photometry of the PS1-discovered Quasars Selected as *i*-dropouts with $i_{P1} - z_{P1} \geqslant 0.5$ ($6.2 \lesssim z \lesssim 6.5$)

Quasar	z	Photometry (mag)
P009–10	5.95	$i_G > 23.39$ $z_G = 21.11 \pm 0.06$ $J_G = 19.93 \pm 0.07$
		$H_G = 19.72 \pm 0.11$
P065–26	6.14	$i_G = 22.70 \pm 0.17$ $z_G = 20.30 \pm 0.03$
		$J_G = 19.32 \pm 0.06$ $H_G = 19.39 \pm 0.18$
		$I_E = 22.24 \pm 0.07$
P159–02	6.38	$I_E > 23.74$ $J_S = 20.00 \pm 0.10$
P210+27	6.14	$Y = 20.93 \pm 0.20$ $J = 20.35 \pm 0.15$ (UKIDSS)
P217–16	6.11	$I_E = 22.53 \pm 0.06$ $Z_E = 20.44 \pm 0.03$
		$Y_{O2K} > 18.43$ $J_{O2K} = 19.69 \pm 0.07$
P217–07	6.14	$i_G = 23.58 \pm 0.28$ $z_G = 21.05 \pm 0.03$
		$J_G = 19.62 \pm 0.09$
P308–21	6.24	$i_G > 23.60$ $z_G = 20.98 \pm 0.05$ $J_G = 20.17 \pm 0.11$
P333+26	6.03	$I_E = 22.48 \pm 0.17$ $Z_E = 20.58 \pm 0.07$
		$J_S = 20.40 \pm 0.13$ $J_{SWIRC} = 20.44 \pm 0.05$

Note. Quasars sorted by right ascension. Their complete names and coordinates are given in Table 7. Their PS1 magnitudes are listed in Table 8. Note that even when these quasars were selected with $z_{P1} - y_{P1} \geqslant 0.5$, most of them have a lower redshift than expected (i.e., $z < 6.2$).

(This table is available in its entirety in machine-readable form.)

Table 4
Follow-up Photometry of the PS1-discovered Quasars that do not Satisfy all Our Selection Criteria

Quasar	z	Photometry (mag)
P000+26	5.75	$z_{O2K} = 19.49 \pm 0.01$ $J_{O2K} = 19.53 \pm 0.02$
P089–15	6.05	$i_G = 23.27 \pm 0.20$ $z_G = 19.94 \pm 0.02$
		$J_G = 19.17 \pm 0.04$ $H_G = 18.47 \pm 0.04$
		$Y_R = 19.68 \pm 0.04$
P108+08	5.92	$i_G = 22.34 \pm 0.14$ $z_G = 19.35 \pm 0.02$
		$J_G = 19.29 \pm 0.06$ $H_G = 19.03 \pm 0.07$
P135+16	5.63	$i_G = 22.70 \pm 0.18$ $z_G = 20.85 \pm 0.04$
		$J_G = 20.30 \pm 0.12$; $H_G = 20.91 \pm 0.33$
P245–00	5.68	$i_G > 23.49$ $z_G = 21.69 \pm 0.09$ $J_G = 20.78 \pm 0.22$
		$Y_R = 21.30 \pm 0.13$ $J_R = 21.10 \pm 0.19$

Note. Quasars sorted by right ascension. Their complete names and coordinates are given in Table 7. Their PS1 magnitudes are listed in Table 8. These quasars were selected according to the extended PS1 criteria, and they are discussed in Section 4.3.

(This table is available in its entirety in machine-readable form.)

5. THE PS1 DISTANT QUASAR SAMPLE

At the time of writing (2016 March) there are 173 known quasars at $z > 5.6$. We provide their names, coordinates, and redshifts in Table 7 and their PS1 PV3, *J*-band, and *WISE* magnitudes in Table 8. The PS1 PV3 catalog has information for about 81% of these quasars, with at least 5σ detections in the z_{P1} or y_{P1} bands. The selection criteria presented in Section 2 and Venemans et al. (2015a) recover 119 of these quasars plus five PS1-discovered quasars that were selected by extended criteria (see Section 4.3). Thus, the PS1 distant quasar sample currently consists of 124 quasars at $z > 5.6$, encompassing more than 70% of the quasars known at these redshifts.

Figure 8 shows the redshift and UV luminosity distribution of all known quasars at $z > 5.6$, highlighting the PS1 distant quasar sample in red.

The sky distribution of all quasars at $z > 5.6$ is presented in Figure 9. We see that a large fraction of the new PS1 discoveries are located in the southern sky. There are seven known quasars at decl. $< -30°$, which were not recovered by our search since they fall outside of the PS1 footprint. The seven quasars at decl. $< -30°$ were discovered by Carnall et al. (2015), Reed et al. (2015), and Venemans et al. (2013, 2015b) using the VST-ATLAS, DES, and VIKING and KiDS surveys, respectively.

Table 5
Spectroscopic Observations of the New PS1 Quasars

Quasar	Date	Telescope/Instrument	Exposure Time	Slit Width
PSO J000.3401+26.8358	2014 Oct 19	MMT/Red Channel	300 s	1.″0
	2015 Nov 5	VLT/FORS2	1500 s	1.″0
PSO J002.1073–06.4345	2013 Oct 24	VLT/FORS2	1482 s	1.″3
PSO J002.3786+32.8702	2014 Dec 23	P200/DBSP	1800 s	1.″5
PSO J004.3936+17.0862	2016 Feb 3	LBT/MODS	2700 s	1.″2
PSO J004.8140–24.2991	2013 Aug 10	*Magellan*/FIRE	2409 s	0.″6
	2014 Oct 12	VLT/FORS2	1452 s	1.″3
PSO J007.0273+04.9571	2013 Jul 9	VLT/FORS2	1782 s	1.″3
PSO J009.3573–08.1190	2015 Dec 4	Keck I/LRIS	600 s	1.″0
PSO J009.7355–10.4316	2014 Oct 28	VLT/FORS2	1362 s	1.″3
PSO J021.4213–25.8822	2014 Nov 16	VLT/FORS2	1370 s	1.″3
PSO J023.0071–02.2675	2013 Oct 25	MMT/Red Channel	600 s	1.″25
PSO J025.2376–11.6831	2013 Oct 26	MMT/Red Channel	1800 s	1.″25
PSO J029.5172–29.0886	2013 Nov 27	VLT/FORS2	1482 s	1.″3
PSO J036.5078+03.0498	2014 Jul 25	NTT/EFOSC2	7200 s	1.″2
	2014 Sep 4–6	*Magellan*/FIRE	8433 s	0.″6
	2014 Oct 20	Keck I/LRIS	1800 s	1.″0
	2015 Dec 28–31	VLT/FORS2	4000 s	1.″0
PSO J037.9706–28.8389	2013 Mar 4–5	VLT/FORS2	3600 s	1.″3
PSO J040.0159+17.5458	2014 Oct 19	MMT/Red Channel	1200 s	1.″0
	2015 Dec 31	VLT/FORS2	1500s	1.″0
PSO J042.6690–02.9174	2013 Oct 25	MMT/Red Channel	1800 s	1.″25
PSO J045.1840–22.5408	2013 Aug 9	VLT/FORS2	1782 s	1.″3
PSO J049.2934–26.5543	2016 Mar 11	*Magellan*/LDSS3	600 s	1.″0
PSO J053.9605-15.7956	2016 Feb 5	P200/DBSP	3600 s	1.″5
PSO J055.4244–00.8035	2014 Feb 22	P200/DBSP	2400 s	1.″5
	2014 Aug 4	VLT/FORS2	1467 s	1.″3
PSO J056.7168–16.4769	2013 Oct 25	MMT/Red Channel	1800 s	1.″25
PSO J060.5529+24.8567	2015 Feb 17	P200/DBSP	2700 s	1.″5
PSO J065.4085–26.9543	2014 Mar 6	NTT/EFOSC2	3600 s	1.″5
	2014 Aug 4	VLT/FORS2	1467 s	1.″3
PSO J065.5041–19.4579	2014 Dec 23	P200/DBSP	1800 s	1.″5
PSO J071.0322–04.5591	2015 Dec 1	MMT/Red Channel	3600 s	1.″0
PSO J071.4507–02.3332	2013 Oct 4	*Magellan*/FIRE	1818 s	0.″6
	2013 Oct 12	CAHA 3.5 m/TWIN	7200 s	1.″2
PSO J075.9356–07.5061	2013 Oct 26	MMT/Red Channel	2400 s	1.″25
PSO J089.9394–15.5833	2015 Dec 4	Keck I/LRIS	900 s	1.″0
PSO J108.4429+08.9257	2015 Dec 4	Keck I/LRIS	900 s	1.″0
PSO J127.2817+03.0657	2014 Dec 23	P200/DBSP	2700 s	1.″5
PSO J135.3860+16.2518	2014 Mar 3	NTT/EFOSC2	3600 s	1.″5
	2014 Apr 5	LBT/MODS	2400 s	1.″2
	2014 Apr 26	VLT/FORS2	1467 s	1.″3
PSO J135.8704–13.8336	2014 Dec 23	P200/DBSP	1800 s	1.″5
PSO J157.9070–02.6599	2015 Mar 14	MMT/Red Channel	900 s	1.″0
PSO J159.2257–02.5438	2015 Mar 14	MMT/Red Channel	900 s	1.″0
	2016 Jan 10	VLT/FORS2	1500 s	1.″0
PSO J167.4726+56.9521	2015 Mar 16	MMT/Red Channel	1200 s	1.″0
PSO J167.6415–13.4960	2014 Apr 26	VLT/FORS2	2630 s	1.″3
	2014 May 30–Jun 2	*Magellan*/FIRE	12004 s	0.″6
PSO J172.1770+26.8866	2015 Mar 16	MMT/Red Channel	2400 s	1.″0
PSO J174.7920–12.2845	2015 May 10	MMT/Red Channel	1800 s	1.″0
	2015 May 12	VLT/FORS2	1500 s	1.″3
PSO J175.4091–20.2654	2016 Feb 5	P200/DBSP	2400 s	1.″5
PSO J178.5594–12.1881	2016 Feb 5	P200/DBSP	3600 s	1.″5
PSO J183.2991–12.7676	2013 Apr 13	VLT/FORS2	1782 s	1.″3
	2013 Apr 19	*Magellan*/FIRE	6000 s	0.″6
PSO J184.3389+01.5284	2016 Feb 4	LBT/MODS	2700 s	1.″2
PSO J187.1047–02.5609	2014 Mar 9	MMT/Red Channel	1800 s	1.″0
	2015 May 8	VLT/FORS2	1500 s	1.″3
PSO J187.3050+04.3243	2013 Apr 12	VLT/FORS2	2682 s	1.″3
PSO J194.1290+25.5476	2016 Feb 14	Keck/LRIS	900 s	1.″5

Table 5
(Continued)

Quasar	Date	Telescope/Instrument	Exposure Time	Slit Width
PSO J197.7198+25.5351	2016 Feb 14	Keck/LRIS	900 s	1.″5
PSO J201.9222+57.5440	2015 May 9	MMT/Red Channel	900 s	1.″0
PSO J209.2058–26.7083	2014 Apr 22	VLT/FORS2	1482 s	1.″3
PSO J210.7277+40.4008	2015 Feb 17	P200/DBSP	1800 s	1.″5
PSO J210.4472+27.8263	2015 May 10	MMT/Red Channel	1800 s	1.″0
PSO J210.8296+09.0475	2015 Mar 14	MMT/Red Channel	1800 s	1.″0
PSO J210.8722–12.0094	2013 May 9	VLT/FORS2	2682 s	1.″3
PSO J212.2974–15.9865	2016 Jan 15	VLT/FORS2	1500 s	1.″0
PSO J213.3629–22.5617	2013 May 3	VLT/FORS2	1782 s	1.″3
PSO J213.7329–13.4803	2015 May 12	VLT/FORS2	1500 s	1.″3
PSO J215.1514–16.0417	2011 Mar 12–13	MMT/Red Channel	2700 s	1.″0
	2011 Apr 9–12	CAHA 3.5 m/TWINS	4800 s	1.″5
	2011 May 28	LBT/LUCI	4800 s	1.″0
PSO J217.0891–16.0453	2014 Apr 22	VLT/FORS2	1467 s	1.″3
PSO J217.9185–07.4120	2016 Mar 12	*Magellan*/LDSS3	1200 s	1.″0
PSO J228.6871+21.2388	2015 Feb 17	P200/DBSP	1800 s	1.″5
PSO J235.9450+17.0079	2014 Jul 21	P200/DBSP	1200 s	1.″5
PSO J236.2912+16.6088	2015 Mar 16	MMT/Red Channel	2400 s	1.″0
	2015 Mar 20	VLT/FORS2	1422 s	1.″3
PSO J238.8510–06.8976	2015 Jun 6	LBT/MODS	1800 s	1.″2
PSO J239.7124–07.4026	2015 May 9	MMT/Red Channel	1200 s	1.″0
	2015 May 17	VLT/FORS2	1500 s	1.″3
PSO J242.4397–12.9816	2014 Mar 9	MMT/Red Channel	1800 s	1.″0
	2015 May 16	VLT/FORS2	1500 s	1.″3
PSO J245.0636–00.1978	2015 Jun 14	LBT/MODS	2700 s	1.″2
PSO J267.0021+22.7812	2015 Apr 13	VLT/FORS2	1500 s	1.″3
PSO J293.0317+71.6523	2015 May 9	MMT/Red Channel	1800 s	1.″0
PSO J308.0416–21.2339	2014 Oct 10	VLT/FORS2	1362 s	1.″3
PSO J308.4829–27.6485	2013 Oct 1	*Magellan*/FIRE	3001 s	0.″6
	2015 May 16	VLT/FORS2	1500 s	1.″3
PSO J319.6040–10.9326	2013 Oct 25	MMT/Red Channel	1800 s	1.″25
PSO J320.8703–24.3604	2013 Oct 21	VLT/FORS2	1482 s	1.″3
PSO J328.7339–09.5076	2015 Aug 9	P200/DBSP	2400 s	1.″5
	2015 Aug 13	Keck/LRIS	900 s	1.″5
PSO J333.9859+26.1081	2015 Aug 13	Keck/LRIS	900 s	1.″5
PSO J338.2298+29.5089	2014 Oct 19	MMT/Red Channel	1800 s	1.″0
	2014 Oct 30	*Magellan*/FIRE	7200 s	0.″6
	2014 Nov 27	LBT/MODS	2700 s	1.″2
	2014 Dec 6	LBT/LUCI	3360 s	1.″5
PSO J340.2041–18.6621	2012 Jun 21	NTT/EFOSC2	3600 s	1.″5
	2012 Nov 17	LBT/MODS	3000 s	1.″2
PSO J357.8289+06.4019	2015 Aug 25	VLT/FORS2	1500 s	1.″3
PSO J359.1352–06.3831	2014 Oct 19	MMT/Red Channel	600 s	1.″0

Note. Quasars sorted by right ascension. For full coordinates and redshifts, see Table 7. The 14 PS1 quasars published in Morganson et al. (2012), Bañados et al. (2014, 2015b), and Venemans et al. (2015a) are included here for completeness.

There are 13 other known quasars. However, even though they have information in the PS1 database, they do not satisfy our S/N requests, or their i_{P1} images are too shallow to satisfy our color cuts (SDSS J0129–0035, CFHQS J0136+0226, CFHQS J0316–1340, CFHQS J1059–0906, VIK J1148+0056, CFHQS J1429+5447, SDSS J2053+0047, CFHQS J2229+1457, SDSS J2307+0031, CFHQS J2318–0246, CFHQS J2329–0301, SDSS J2356+0023). We did not select SDSS J1621+5155 ($z = 5.71$) given its $i_{P1} - z_{P1} = 1.85$ color, although it does satisfy our $y_{P1} - J$ requirement and all of our *WISE* prioritization criteria (see Figures 4 and 5). ULAS J1120+0641 ($z = 7.08$) is a special case as it does not appear in the PS1 PV3 catalog. Forced photometry on the PV3 y_{P1} image yielded a 4.3σ detection with $y_{P1} = 21.31 \pm 0.25$. This is significantly fainter than what we expected from its published photometry. This would not be the first time that a possible flux decrement has been suggested for this object. Simpson et al. (2014) reported that the *Hubble Space Telescope* (*HST*) photometry of this quasar was 14% (19%) fainter in the F105W (F125W) filter than expected from its discovery spectrum and photometry (Mortlock et al. 2011). We recently re-observed this quasar in the Y and J bands with the RetroCam instrument at the du Pont telescope in Las Campanas Observatory. The observations were carried out on 2016 March 30, and the total exposure times were 1200 s. The measured magnitudes are $Y_R = 20.36 \pm 0.06$ and $J_R = 20.36 \pm 0.05$. While these magnitudes are fainter than the reported magnitudes for this quasar ($Y = 20.26 \pm 0.04$, $J = 20.16 \pm 0.07$; Barnett et al. 2015), the differences are not significant ($\lesssim 2\sigma$).

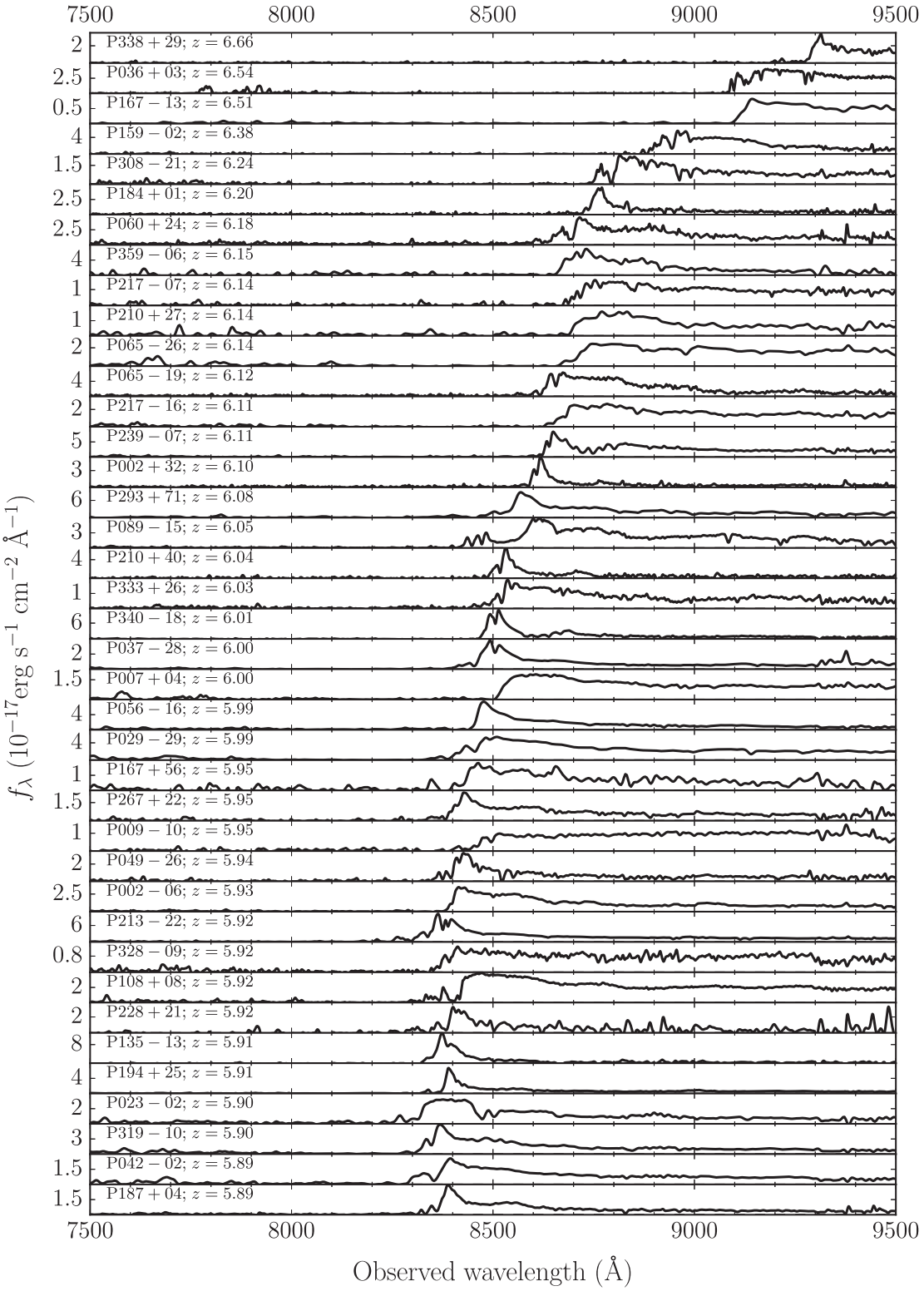

Figure 7. Spectra of the 77 Pan-STARRS1 discovered quasars at $z \geqslant 5.6$. Sorted by decreasing redshift.

6. PS1 QUASAR COMPOSITE SPECTRUM

Fan et al. (2004) presented the first quasar composite spectrum at $z \sim 6$. This composite consisted of 12 SDSS quasars at $z > 5.7$ and showed no clear differences in spectral properties relative to quasars at $z \sim 2$ (see their Figure 3). With our much enlarged sample of quasars at $z > 5.6$, we have an opportunity to revisit this issue by creating composite spectra of our quasar sample as well as of subsamples with different emission line properties.

The black line in Figure 10 shows the composite spectrum of 117 $z > 5.6$ quasars from the PS1 sample. These spectra include all 77 PS1-discovered quasars plus other spectra kindly

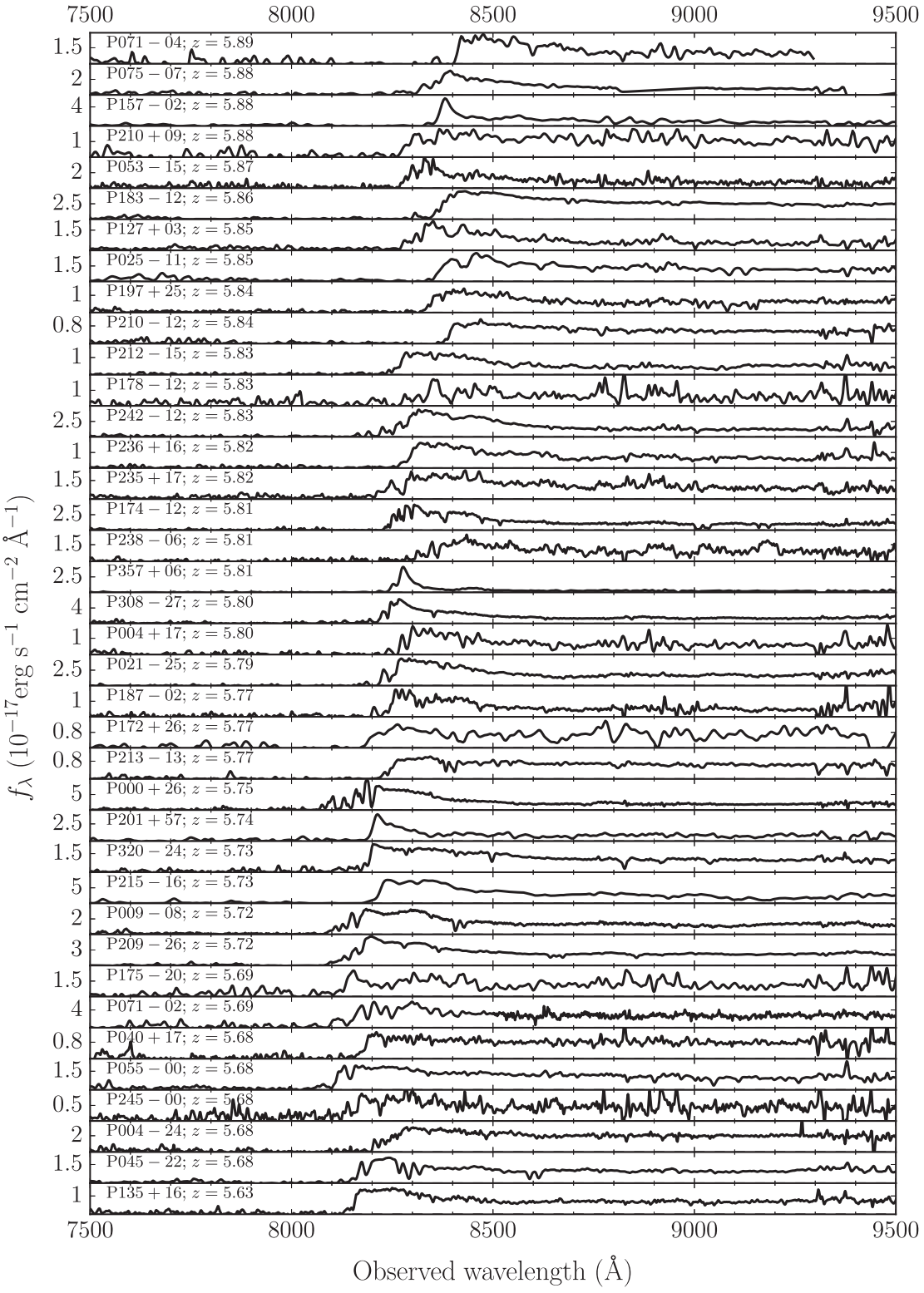

Figure 7. (Continued.)

provided by the authors of their discovery papers. In order to create the composite, we first normalized every individual spectrum to its median flux in the rest-frame wavelength range 1285–1295 Å, which is a region free of emission lines (e.g., Vanden Berk et al. 2001). Next, we resampled the spectra to a common wavelength grid and combined them using a simple arithmetic median, which preserves the relative fluxes of emission lines (Vanden Berk et al. 2001). As can be seen from Figure 10, redward of Lyα the composite spectrum agrees fairly well with the low-redshift composite spectrum of bright ($r \lesssim 17$) $1.0 < z < 2.1$ quasars from Selsing et al. (2016) (gray dashed line). Blueward of Lyα the emission is virtually zero

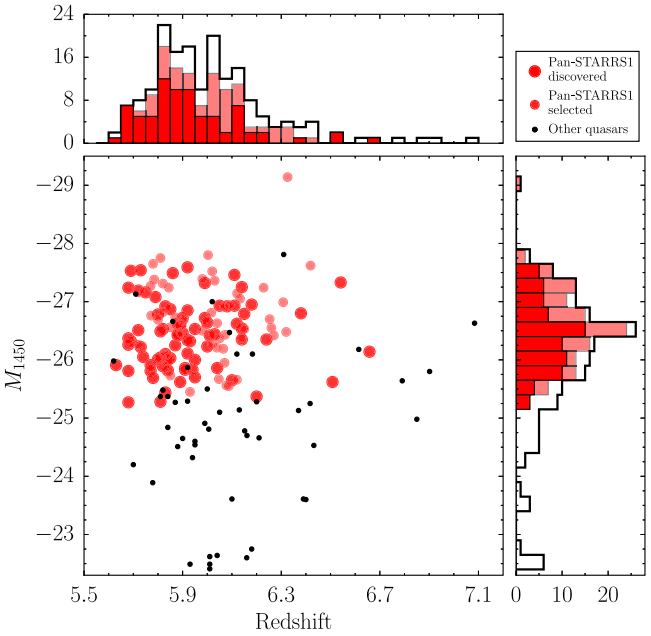

Figure 8. Redshift and absolute UV magnitude (M_{1450}) distribution of all known $z > 5.6$ quasars as of 2016 March.

due to the strong intergalactic medium (IGM) absorption at these redshifts.

We created two additional composite spectra following the same procedure as above: one from 10% of the spectra with the largest rest-frame Lyα + N V equivalent width (EW (Lyα + N V)) values and the other from 10% of the spectra with the smallest EW(Lyα + N V) values. In order to estimate the EWs of our quasar sample, we followed the procedure of Diamond-Stanic et al. (2009). In short, we fit a power law of the form $f_\lambda = C \times \lambda^\beta$ to regions usually free of emission lines (1285–1295, 1315–1325, 1340–1375, 1425–1470, 1680–1710, 1975–2050, and 2150–2250 Å). We then obtained the EW by integrating the flux above the continuum between $\lambda_{\rm rest} = 1160$ Å and $\lambda_{\rm rest} = 1290$ Å. However, as discussed in Section 4.2, it was challenging to obtain a robust fit of the continuum for most of our spectra. Therefore, to circumvent this difficulty, we fixed the power law index β. We estimated the EWs using two different power-law indices: $\beta = -1.5$ (Vanden Berk et al. 2001) and $\beta = -1.7$ (Selsing et al. 2016). Finally, we averaged these EWs.

The two composite spectra with the strong and weak emissions are shown in Figure 10 with red and blue lines, respectively. The differences are quite evident: on the one hand, the first composite spectrum shows a much stronger Lyα line than the composite of low-redshift bright quasars; on the other hand, the Lyα line in our second composite spectrum is virtually absent and resembles a weak-emission line quasar (see Section 7). We note that, in general, redshift uncertainties are larger for weak-lined objects, which might blur out emission features in a composite spectrum even more. The mean redshift and M_{1450} of the quasars used for the composite spectra with strong and weak emissions are $(6.05 \pm 0.11;\ -26.28 \pm 0.49)$ and $(5.91 \pm 0.18;\ -27.03 \pm 0.88)$, respectively.

The three composite spectra created in this section are available in Table 6.

7. WEAK EMISSION LINE QUASARS

Diamond-Stanic et al. (2009) studied a sample of ~3000 quasars in the redshift range $3 < z < 5$. They found that the distribution of EW(Lyα + N V) follows a log-normal distribution, and defined weak-line quasars as the 3σ outliers at the low-end of this distribution, i.e., EW < 15.4 Å. This study also showed that the fraction of weak-line quasars evolves with redshift, increasing from 1.3% at $z < 4.2$ to 6.2% at $z > 4.2$.

It has been argued that the fraction of weak-line quasars at $z \sim 6$ could reach ~25%, i.e., they are much more abundant than the 1%–6% fraction observed at lower redshifts (Bañados et al. 2014). Several scenarios have been proposed to explain the existence of these intriguing weak-line quasars, but no consensus has been reached (e.g., Laor & Davis 2011; Wu et al. 2012; Wang et al. 2014; Luo et al. 2015; Shemmer & Lieber 2015). A large fraction of weak-line quasars at the highest accessible redshifts could support evolutionary scenarios suggesting that these rare quasars may be in such an early formation phase that their broad-line region is not yet in place (Liu & Zhang 2011). We will revisit this issue with the 117 $z > 5.6$ PS1 quasars used in Section 6.

Figure 11 shows the distribution of the EW(Lyα + N V) of the PS1 sample, as estimated in Section 6. Of these quasars, 13.7% (16/117) satisfy the weak-line quasar definition of Diamond-Stanic et al. (2009). Even though this fraction is larger than what is found at lower redshifts, it is significantly lower than our initial discoveries suggested (Bañados et al. 2014).

In Figure 12 we show the log-normal distribution best fit to our data, with $\langle \log \text{EW (Å)} \rangle = 1.542$ and $\sigma(\log \text{EW (Å)}) = 0.391$ (blue line). In comparison with the best-fit distribution found by Diamond-Stanic et al. (2009) (yellow dashed line), our best-fit distribution peaks at lower EWs and has a larger dispersion. These two effects could be explained due to the increased opacity of the IGM at $z > 5.6$. The Lyα line at $z > 5.6$ is, on average, more absorbed than in the quasars studied by Diamond-Stanic et al. (2009). As a simple test, we measure the EW(Lyα + N V) of the original Vanden Berk et al. (2001) and Selsing et al. (2016) templates and of modified versions where all the flux shortward of Lyα is set to zero. The differences between the two versions are 15.0 ± 5.8 Å and 26.8 ± 6.74 Å for the Vanden Berk et al. (2001) and Selsing et al. (2016) templates, respectively. These differences are comparable with the overall mean shift of 28.7 Å found between the EW(Lyα + N V) distributions of Figure 12. Alternatively, it could be that the EW distributions are actually different, in which case we would need to reconsider the definition of a weak-line quasar. For instance, the lower 3σ cut of our best-fit distribution is <2.3 Å, which is very different from the 15.4 Å found by Diamond-Stanic et al. (2009). It would be interesting to test whether there is an evolution of EW(Lyα + N V) distribution with redshift, in addition to the weak-line fraction evolution.

An important point is the impact of selection effects, since quasar color selection is significantly affected by the strength of the Lyα emission line. Figure 13 shows the redshift versus $i_{\rm P1} - z_{\rm P1}$ and $z_{\rm P1} - y_{\rm P1}$ color tracks for the composite spectra of Section 6. It is clear that at $5.65 < z < 5.75$ we are biased to find more quasars with weaker Lyα, while at $z > 6.2$ these weak-line quasars are hard to select. Coincidentally, the redshift range $5.75 < z < 6.00$ is where we are sensitive to selecting both quasars with strong Lyα and those with weak Lyα, and also corresponds to the color selection region where

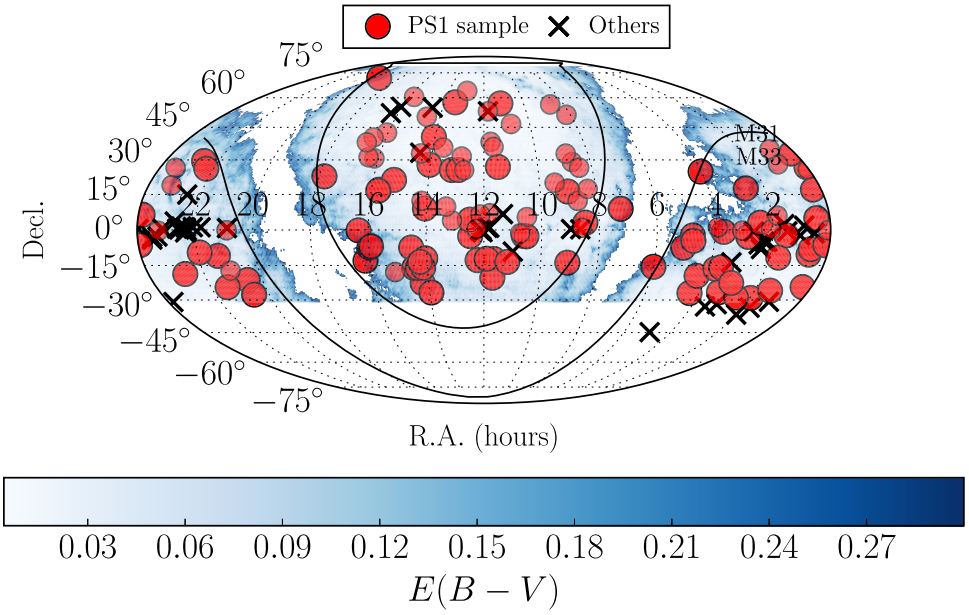

Figure 9. Sky distribution of all known $z > 5.6$ quasars. Red circles represent the PS1 distant quasar sample. Larger symbols are PS1 discoveries. Black crosses are quasars that do not belong to the PS1 distant quasar sample. The solid lines show the border of the Milky Way plane traditionally avoided by high-redshift quasar surveys ($|b| < 20°$). The locations of M31 and M33 are also indicated. The color map shows the $E(B-V)$ reddening map in the PS1 footprint (decl. $> -30°$) from Schlegel et al. (1998), where $E(B-V) < 0.3$. Note that we discovered two quasars with $|b| < 20°$ in regions with low extinction.

our follow-up is more complete. The weak-line fraction of quasars in this redshift range is 12.1% (7/58), consistent with the estimate based on the whole sample considering Poisson errors. We note that quasars with weak Lyα are in general closer to our selection boundaries and thus more prone to be missed in comparison to quasars with normal or strong Lyα. For example, the $z = 5.71$ quasar J1621+5155 with EW(Lyα + N v) < 5 Å (Wang et al. 2008) is not part of the PS1 distant quasar sample merely because of its $i_{\rm P1} - z_{\rm P1} = 1.85 \pm 0.07$ color. Therefore, quasars with a weak Lyα line have higher incompleteness in our sample, and as a consequence, it is likely that the fraction of weak-line quasars is underestimated.

Our current high-redshift sample seems to confirm a larger fraction of quasars with weak emission lines if we use the definition of Diamond-Stanic et al. (2009). However, we note that the EW distribution we find is significantly different from the one reported by Diamond-Stanic et al. (2009; Figure 12), which might have consequences on what we call a weak-line quasar. We caution that the results of this section are mainly based on the Lyα line, which is complicated and particularly challenging to interpret at the end of cosmic reionization. It is then critical to test the fraction of weak-line quasars by studying other strong broad emission lines, such as C IV and Mg II (see, e.g., Plotkin et al. 2015) in order to make sure that the evolution we see is not only due to the increase of the IGM neutral fraction with redshift. We will therefore postpone a more thorough analysis of the fraction of weak-line quasars until we obtain near-infrared spectroscopy for a representative sample of our quasars. This effort is currently underway.

8. SUMMARY AND CONCLUSIONS

One of the key challenges for modern astronomy is studying and understanding the earliest sources and structures of the universe—their formations and evolutions across cosmic time. Luminous quasars at the highest accessible redshifts are ideal tools for probing the early universe. However, strong conclusions from their study have previously been limited by low-number statistics.

In this paper, we describe our method to identify quasars in the redshift range $5.6 \lesssim z \lesssim 6.5$ by mining the Pan-STARRS1 database (Section 2) complemented by follow-up optical and near-infrared observations (Section 3). This is an update to the criteria presented in Bañados et al. (2014) and complements our method to find quasars at $z \gtrsim 6.5$ described in Venemans et al. (2015a). In total, we have so far discovered 77 quasars at $5.6 \lesssim z \lesssim 6.7$ (63 new discoveries presented in this paper; see Section 4), almost doubling the previously known number of quasars within the first gigayear of the universe (see Figure 7). It is important to note that a large fraction of these newly discovered quasars are in the southern sky (see Figure 9), which constitutes the ideal ground for follow-up investigations using facilities such as ALMA, VLT, and the *Magellan* Telescopes.

Our search is still ongoing and now uses the latest data release of the Pan-STARRS1 survey, which has only recently been made available. In the short term, we plan to mine this more detailed data set to complete a more homogeneous quasar sample at $5.75 < z < 6.00$, which can be used to provide an updated $z \sim 6$ quasar luminosity function, more accurate than what was possible with previous, smaller quasar samples. We are currently working to understand and model the selection function and completeness of our survey. The challenge is to take into account the inhomogeneous depth of different bands across the sky (Figure 2) and the big impact that diverse emission line properties have on our selection (Figure 13); thus, rigorous modeling is needed. We will eventually use this modeling work to also constrain the quasar luminosity function at higher redshifts, where the discovery of more quasars is imminent.

In Section 5, we introduce the PS1 distant quasar sample, which currently consists of 124 quasars that satisfy our

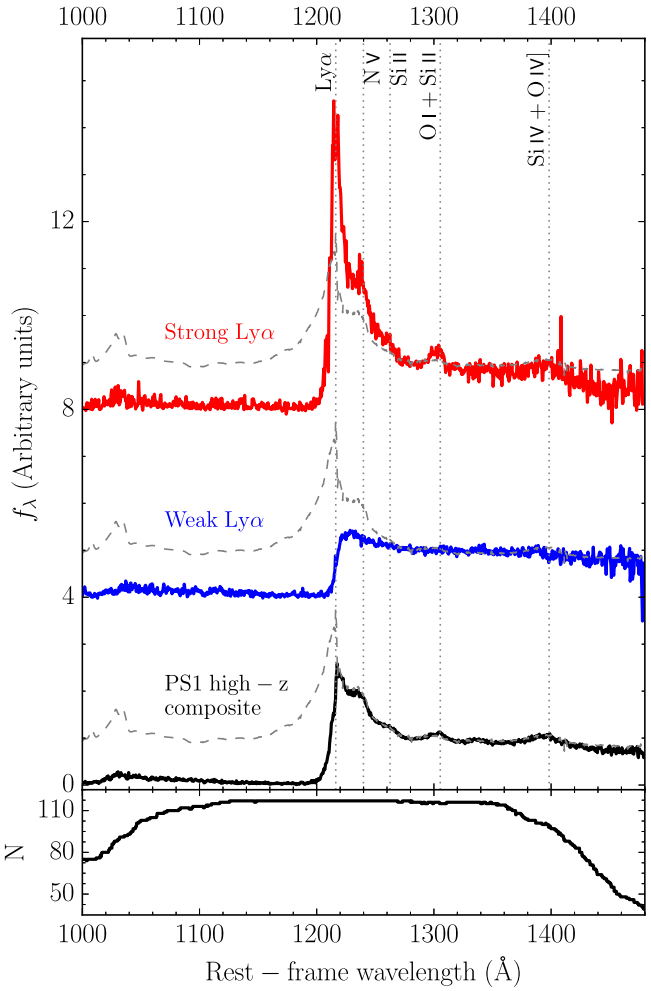

Figure 10. Top: arithmetic median composite spectrum of 117 quasars belonging to the PS1 sample is shown in black. The gray dashed line is the low-redshift composite quasar spectrum from Selsing et al. (2016) for comparison. The blue (red) line is the composite spectrum determined from 10% of individual spectra with the weakest (strongest) EW(Lyα + N V). The blue and red spectra are vertically shifted by 4 and 8 units, respectively. Bottom: number of quasars per wavelength bin contributing to the PS1 high-redshift quasar composite spectrum (black line on the top panel). These composite spectra show the diversity of the PS1 quasars in terms of their emission line properties. The $z > 5.6$ PS1 quasar composite spectrum is available from the online journal (in Table 6).

Table 6
PS1 Distant Quasar Sample Arithmetic Median Composite Spectra (see Figure 10)

λ Å	$f_{\lambda,\mathrm{all}}$	N	$f_{\lambda,\mathrm{strong}}$	$f_{\lambda,\mathrm{weak}}$
1000.0	0.031	75	0.020	0.038
1000.5	0.043	75	0.039	0.075
1001.0	0.057	75	0.036	0.139
1001.5	0.053	75	0.011	0.145
1002.0	0.055	75	0.017	0.221
1002.5	0.080	75	0.007	0.145
1003.0	0.045	75	−0.027	0.083
1003.5	0.039	74	0.094	0.065
1004.0	0.054	74	0.144	0.075
1004.5	0.031	75	0.028	0.071

(This table is available in its entirety in machine-readable form.)

selection criteria, while a complete census of all quasars currently known at $z > 5.6$ is provided in Appendix A. Composite spectra of the PS1 quasar sample are presented in Section 6. The PS1 distant quasar sample spans a large range of redshifts and luminosities (see Figure 8) and shows a broad variety of spectral features, including quasars with very strong Lyα emission and others with weak or completely absorbed Lyα (see Figures 7 and 10).

In Section 7, we revisit the issue of how common weak emission line quasars are at high redshift. Following Diamond-Stanic et al. (2009), we find that 13.7% of our quasars are weak-line quasars (Figure 11), a larger fraction than what is found at lower redshifts. However, we note that these results are based mostly on Lyα and the weak-line classification for some of these quasars is not irrefutable (see Figure 12). Therefore, near-infrared spectroscopy of this sample is required to establish whether some of these objects are real weak-line quasars or their Lyα is significantly affected by the neutral IGM (see, e.g., Figure 3 in Bañados et al. 2014).

So far, most studies of high-redshift quasars have focused on individual objects or a few sources. The coming years should see a vast improvement of our understanding of the early universe through studies of the distant quasar population presented in this work. This will require a combined and dedicated effort of X-ray, optical, (near-)infrared, (sub-) millimeter, and radio observations using the current and next generation of ground- and space-based telescopes. Moreover, the upcoming surveys and facilities will enable us to find fainter quasars and push the redshift frontier even further. To conclude, the large number of quasars presented in this paper is merely the start of an exciting transition era toward a statistical characterization of the earliest massive black holes and galaxies in the universe.

We acknowledge the assistance of the following people in some of the observations presented herein: Roberto Assef, Carla Fuentes, David Girou, Fiona Harrison, Bing Jiang, George Lansbury, Elena Manjavacas, Alejandra Melo, Gaël Noirot, Michael Rauch, and Eden Stern. We also thank Carlos Contreras for his help with the data reduction of the near-infrared images taken with Retrocam at the du Pont Telescope. EPF and BPV acknowledge funding through the ERC grant "Cosmic Dawn." XF, IM, and JTS acknowledge support from NSF grants AST 11-07682 and AST 15-15115. ES acknowledges support for this work provided by NASA through Hubble Fellowship grant HST-HF2-51367.001-A, awarded by the Space Telescope Science Institute, which is operated by the Association of Universities for Research in Astronomy, Inc., for NASA, under contract NAS 5-26555.

The Pan-STARRS1 Surveys (PS1) have been made possible through contributions of the Institute for Astronomy, University of Hawaii; the Pan-STARRS Project Office; the Max Planck Society and its participating institutes (the Max Planck Institute for Astronomy, Heidelberg, and the Max Planck Institute for Extraterrestrial Physics, Garching); the Johns Hopkins University; Durham University; the University of Edinburgh; Queen's University Belfast; the Harvard–Smithsonian Center for Astrophysics; the Las Cumbres Observatory Global Telescope Network, Incorporated; the National Central University of Taiwan; the Space Telescope Science Institute; the National Aeronautics and Space Administration (under Grant No. NNX08AR22G, issued through the Planetary

Table 7
All $z > 5.6$ Quasars Known as of 2016 March

Quasar	R.A. (J2000)	Decl. (J2000)	z	Method [a]	m_{1450} [b] (mag)	M_{1450} (mag)	PS1 [c]	References disc./z/m_{1450}
PSO J000.3401+26.8358	00:01:21.63	+26:50:09.17	5.75	4	19.52	−27.16	4	1/1/1
SDSS J0002+2550	00:02:39.39	+25:50:34.96	5.82	3	19.39	−27.31	1	5/22/1
SDSS J0005–0006	00:05:52.34	−00:06:55.80	5.85	2	20.98	−25.73	1	5/12/1
PSO J002.1073–06.4345	00:08:25.77	−06:26:04.42	5.93	4	20.41	−26.32	1	1;43/1/1
PSO J002.3786+32.8702	00:09:30.89	+32:52:12.94	6.10	4	21.13	−25.65	1	1/1/1
PSO J004.3936+17.0862	00:17:34.47	+17:05:10.70	5.80	4	20.69	−26.01	1	1/1/1
PSO J004.8140–24.2991	00:19:15.38	−24:17:56.98	5.68	4	19.43	−27.24	1	1/1/1
PSO J007.0273+04.9571	00:28:06.56	+04:57:25.64	6.00	4	20.11	−26.64	1	36;43/1/1
CFHQS J0033–0125	00:33:11.40	−01:25:24.90	6.13	4	21.64	−25.14	0	15/15/1
PSO J009.3573–08.1190	00:37:25.76	−08:07:08.46	5.72	4	20.16	−26.51	1	1/1/1
PSO J009.7355–10.4316	00:38:56.52	−10:25:53.90	5.95	4	20.20	−26.53	2	1/1/1
CFHQS J0050+3445	00:50:06.67	+34:45:21.65	6.253	2	20.11	−26.70	2	24/25/1
CFHQS J0055+0146	00:55:02.91	+01:46:18.30	6.006	1	21.94	−24.81	0	21/49/1
SDSS J0100+2802	01:00:13.02	+28:02:25.92	6.3258	1	17.69	−29.14	2	50/54/1
CFHQS J0102–0218	01:02:50.64	−02:18:09.90	5.95	4	22.14	−24.60	0	21/21/1
VIK J0109–3047	01:09:53.13	−30:47:26.31	6.7909	1	21.30	−25.64	0	33/51/1
PSO J021.4213–25.8822	01:25:41.12	−25:52:56.24	5.79	4	19.61	−27.08	1	1/1/1
SDSS J0129–0035	01:29:58.51	−00:35:39.70	5.7787	1	22.80	−23.89	0	18/34/1
PSO J023.0071–02.2675	01:32:01.70	−02:16:03.11	5.90	4	20.27	−26.46	1	1/1/1
CFHQS J0136+0226	01:36:03.17	+02:26:05.70	6.21	4	22.15	−24.66	0	24/24/1
PSO J025.2376–11.6831	01:40:57.03	−11:40:59.48	5.85	4	19.84	−26.87	1	1/1/1
VST-ATLAS J025.6821–33.4627	01:42:43.73	−33:27:45.47	6.31	4	19.02	−27.81	0	42/42/42
ULAS J0148+0600	01:48:37.64	+06:00:20.06	5.98	2	19.35	−27.39	1	43;56/41/1
PSO J029.5172–29.0886	01:58:04.14	−29:05:19.25	5.99	4	19.42	−27.32	1	1/1/1
VST-ATLAS J029.9915–36.5658	01:59:57.97	−36:33:56.60	6.02	4	19.75	−27.00	0	42/42/42
ULAS J0203+0012	02:03:32.38	+00:12:29.27	5.72	3	20.42	−26.26	1	14/20/1
CFHQS J0210–0456	02:10:13.19	−04:56:20.90	6.4323	1	22.33	−24.53	0	25/35/1
CFHQS J0216–0455 [d]	02:16:27.81	−04:55:34.10	6.01	4	24.27	−22.49	0	21/21/1
CFHQS J0221–0802	02:21:22.71	−08:02:51.50	6.161	2	22.09	−24.70	0	24/25/1
PSO J036.5078+03.0498	02:26:01.87	+03:02:59.42	6.5412	1	19.55	−27.33	3	47/40/1
CFHQS J0227–0605	02:27:43.29	−06:05:30.20	6.20	4	21.52	−25.28	0	21/21/1
PSO J037.9706–28.8389	02:31:52.96	−28:50:20.08	6.00	4	20.52	−26.23	1	36/1/1
SDSS J0239–0045	02:39:30.24	−00:45:05.40	5.82	4	21.22	−25.48	0	18/18/1
PSO J040.0159+17.5458	02:40:03.82	+17:32:44.91	5.68	4	20.85	−25.81	1	1/1/1
PSO J042.6690–02.9174	02:50:40.58	−02:55:02.82	5.89	4	20.13	−26.59	1	1/1/1
PSO J045.1840–22.5408	03:00:44.18	−22:32:27.19	5.68	4	20.41	−26.26	1	36/1/1
SDSS J0303–0019	03:03:31.40	−00:19:12.90	6.078	2	21.21	−25.56	1	16/19/1
VIK J0305–3150	03:05:16.92	−31:50:55.90	6.6145	1	20.72	−26.18	0	33/51/1
CFHQS J0316–1340	03:16:49.87	−13:40:32.30	5.99	4	21.84	−24.91	0	24/24/1
PSO J049.2934–26.5543	03:17:10.42	−26:33:15.71	5.94	4	20.91	−25.82	1	1/1/1
VIK J0328–3253	03:28:35.51	−32:53:22.84	5.86	3	20.05	−26.66	0	48/48/1
PSO J053.9605–15.7956	03:35:50.53	−15:47:44.50	5.87	4	20.47	−26.25	1	1/1/1
PSO J055.4244–00.8035	03:41:41.86	−00:48:12.74	5.68	4	20.29	−26.37	1	39/39/1
PSO J056.7168–16.4769	03:46:52.04	−16:28:36.88	5.99	4	20.03	−26.72	1	1/1/1
SDSS J0353+0104	03:53:49.73	+01:04:04.66	6.072	2	20.34	−26.43	1	16/26/1
PSO J060.5529+24.8567	04:02:12.69	+24:51:24.43	6.18	4	19.85	−26.95	1	1/1/1
PSO J065.4085–26.9543	04:21:38.05	−26:57:15.61	6.14	4	19.53	−27.25	2	1/1/1
PSO J065.5041–19.4579	04:22:01.00	−19:27:28.69	6.12	4	20.16	−26.62	1	1/1/1
PSO J071.0322–04.5591	04:44:07.73	−04:33:33.07	5.89	4	20.12	−26.60	1	1/1/1
PSO J071.4507–02.3332	04:45:48.18	−02:19:59.84	5.69	4	19.13	−27.53	1	1/1/1
DES J0454–4448	04:54:01.79	−44:48:31.10	6.09	4	20.30	−26.47	0	46/46/1
PSO J075.9356–07.5061	05:03:44.56	−07:30:22.07	5.88	4	20.10	−26.62	1	1/1/1
PSO J089.9394–15.5833	05:59:45.47	−15:35:00.20	6.05	4	19.83	−26.93	4	1/1/1
PSO J108.4429+08.9257	07:13:46.31	+08:55:32.65	5.92	4	19.14	−27.59	4	1/1/1
SDSS J0810+5105	08:10:54.31	+51:05:40.10	5.82	4	19.88	−26.82	1	55/1/1
SDSS J0818+1722	08:18:27.40	+17:22:52.01	6.02	3	19.24	−27.52	1	8/22/1
ULAS J0828+2633	08:28:13.41	+26:33:55.49	6.05	3	20.40	−26.37	1	56/56/1
PSO J127.2817+03.0657	08:29:07.62	+03:03:56.52	5.85	4	20.68	−26.03	1	1/1/1
SDSS J0836+0054	08:36:43.86	+00:54:53.26	5.81	2	18.95	−27.75	1	3/12/1
VIK J0839+0015	08:39:55.36	+00:15:54.21	5.84	4	21.34	−25.37	0	48/48/48
SDSS J0840+5624	08:40:35.10	+56:24:20.22	5.8441	1	19.46	−27.24	1	8/23/1
SDSS J0841+2905	08:41:19.52	+29:05:04.55	5.98	3	20.24	−26.50	1	9/22/1
SDSS J0842+1218	08:42:29.43	+12:18:50.58	6.069	2	19.86	−26.91	1	26;43/26/1
SDSS J0850+3246	08:50:48.25	+32:46:47.94	5.87	4	19.98	−26.73	1	43/43/1
HSC J0859+0022	08:59:07.19	+00:22:55.90	6.39	3	23.23	−23.62	0	53/53/53
PSO J135.3860+16.2518	09:01:32.65	+16:15:06.83	5.63	4	20.74	−25.91	4	39/39/1
PSO J135.8704–13.8336	09:03:28.91	−13:50:01.27	5.91	4	20.86	−25.86	1	1/1/1
SDSS J0927+2001	09:27:21.82	+20:01:23.64	5.7722	1	19.93	−26.76	1	8/11/1
SDSS J1030+0524	10:30:27.11	+05:24:55.06	6.308	2	19.84	−26.99	1	3/12/1

Table 7
(Continued)

Quasar	R.A. (J2000)	Decl. (J2000)	z	Method [a]	m_{1450} [b] (mag)	M_{1450} (mag)	PS1 [c]	References disc./z/m_{1450}
PSO J157.9070–02.6599	10:31:37.69	−02:39:35.67	5.88	4	20.28	−26.44	1	1/1/1
PSO J159.2257–02.5438	10:36:54.19	−02:32:37.94	6.38	4	20.05	−26.80	2	1/1/1
SDSS J1044–0125	10:44:33.04	−01:25:02.20	5.7847	1	19.31	−27.38	1	2/34/1
SDSS J1048+4637	10:48:45.07	+46:37:18.55	6.2284	1	19.56	−27.24	1	4/22/1
CFHQS J1059–0906	10:59:28.61	−09:06:20.40	5.92	4	20.86	−25.87	0	24/24/1
PSO J167.4726+56.9521	11:09:53.43	+56:57:07.61	5.95	4	20.74	−26.00	1	1/1/1
PSO J167.6415–13.4960	11:10:33.98	−13:29:45.60	6.508	2	21.25	−25.62	3	47/47/1
ULAS J1120+0641	11:20:01.48	+06:41:24.30	7.0842	1	20.38	−26.63	0	27/31/1
PSO J172.1770+26.8866	11:28:42.48	+26:53:12.00	5.77	4	20.78	−25.91	1	1/1/1
SDSS J1137+3549	11:37:17.73	+35:49:56.85	6.03	3	19.40	−27.36	1	8/22/1
PSO J174.7920–12.2845	11:39:10.09	−12:17:04.38	5.81	4	20.20	−26.49	1	1/1/1
PSO J175.4091–20.2654	11:41:38.20	−20:15:55.65	5.69	4	20.35	−26.32	1	1/1/1
SDSS J1143+3808	11:43:38.35	+38:08:28.82	5.80	4	20.01	−26.69	1	55/1/1
ULAS J1148+0702	11:48:03.29	+07:02:08.29	6.32	3	20.35	−26.48	2	56/56/1
RD J1148+5253	11:48:16.21	+52:53:39.30	5.70	4	22.47	−24.20	0	6/6/1
SDSS J1148+5251	11:48:16.65	+52:51:50.39	6.4189	1	19.24	−27.62	3	4/22/1
VIK J1148+0056	11:48:33.18	+00:56:42.26	5.84	3	21.86	−24.84	0	48/48/1
VIK J1152+0055	11:52:21.27	+00:55:36.69	6.37	4	21.71	−25.13	0	53;57/53/1
PSO J178.5594–12.1881	11:54:14.26	−12:11:17.48	5.83	4	20.60	−26.10	1	1/1/1
HSC J1202–0057	12:02:46.37	−00:57:01.70	5.93	4	24.23	−22.50	0	53/53/53
HSC J1205–0000 [e]	12:05:05.10	−00:00:27.97	6.85	4	21.98	−24.98	0	53/53/1
ULAS J1207+0630	12:07:37.44	+06:30:10.24	6.04	4	20.13	−26.63	1	43;56/43/1
HSC J1207–0005 [f]	12:07:54.14	−00:05:53.30	6.01	4	24.13	−22.62	0	53/53/53
PSO J183.2991–12.7676	12:13:11.81	−12:46:03.45	5.86	3	19.22	−27.49	1	36/36/1
VIK J1215+0023	12:15:16.87	+00:23:24.66	5.93	3	21.28	−25.45	1	48/48/1
PSO J184.3389+01.5284	12:17:21.34	+01:31:42.47	6.20	4	21.43	−25.37	1	1/1/1
PSO J187.1047–02.5609	12:28:25.15	−02:33:39.25	5.77	4	20.88	−25.81	1	1/1/1
PSO J187.3050+04.3243	12:29:13.21	+04:19:27.75	5.89	3	21.10	−25.62	1	36/36/1
ULAS J1243+2529	12:43:40.81	+25:29:23.89	5.83	3	20.62	−26.08	1	36;56/56/1
SDSS J1250+3130	12:50:51.93	+31:30:21.90	6.15	3	20.26	−26.53	1	8/22/1
PSO J194.1290+25.5476	12:56:30.97	+25:32:51.45	5.91	4	20.90	−25.83	1	1/1/1
SDSS J1257+6349	12:57:57.48	+63:49:37.16	6.02	4	20.48	−26.27	1	43/43/1
SDSS J1306+0356	13:06:08.27	+03:56:26.36	6.016	2	19.94	−26.81	1	3/12/1
PSO J197.7198+25.5351	13:10:52.75	+25:32:06.68	5.84	4	20.70	−26.00	1	1/1/1
ULAS J1319+0950	13:19:11.30	+09:50:51.52	6.133	1	19.74	−27.05	1	20/34/1
PSO J201.9222+57.5440	13:27:41.32	+57:32:38.37	5.74	4	20.63	−26.05	1	1/1/1
SDSS J1335+3533	13:35:50.81	+35:33:15.82	5.9012	1	20.05	−26.67	1	8/22/1
PSO J209.2058–26.7083	13:56:49.41	−26:42:30.23	5.72	4	19.49	−27.19	1	1/1/1
PSO J210.4472+27.8263	14:01:47.34	+27:49:35.03	6.14	4	20.24	−26.54	2	1/1/1
PSO J210.7277+40.4008	14:02:54.67	+40:24:03.19	6.04	4	20.90	−25.86	1	1/1/1
PSO J210.8297+09.0474	14:03:19.13	+09:02:50.99	5.88	4	20.30	−26.42	1	1;43/1/1
PSO J210.8722–12.0094	14:03:29.33	−12:00:34.14	5.84	4	20.88	−25.82	1	36/36/1
PSO J212.2974–15.9865	14:09:11.38	−15:59:11.66	5.83	4	21.27	−25.44	1	1/1/1
SDSS J1411+1217	14:11:11.29	+12:17:37.28	5.904	2	20.03	−26.69	1	5/12/1
PSO J213.3629–22.5617	14:13:27.12	−22:33:42.25	5.92	4	19.88	−26.85	1	36/1/1
PSO J213.7329–13.4803	14:14:55.90	−13:28:49.28	5.78	4	21.00	−25.69	1	1/1/1
PSO J215.1514–16.0417	14:20:36.34	−16:02:30.25	5.73	3	19.13	−27.54	1	30/30/1
NDWFS J1425+3254	14:25:16.33	+32:54:09.54	5.8918	1	20.25	−26.47	1	7/22/1
FIRST J1427+3312	14:27:38.59	+33:12:42.00	6.12	4	20.68	−26.10	0	10;13/10/1
PSO J217.0891–16.0453	14:28:21.39	−16:02:43.30	6.11	4	19.84	−26.93	2	1/1/1
CFHQS J1429+5447	14:29:52.17	+54:47:17.70	6.1831	1	20.70	−26.10	0	24/28/1
PSO J217.9185–07.4120	14:31:40.45	−07:24:43.47	6.14	4	20.44	−26.35	2	1/1/1
SDSS J1436+5007	14:36:11.74	+50:07:07.16	5.85	3	20.15	−26.56	1	8/22/1
CFHQS J1509–1749	15:09:41.78	−17:49:26.80	6.121	2	19.64	−27.14	1	15/25/1
PSO J228.6871+21.2388	15:14:44.91	+21:14:19.78	5.92	4	20.61	−26.11	1	1/1/1
PSO J235.9450+17.0079	15:43:46.82	+17:00:28.46	5.82	4	20.17	−26.53	1	1/1/1
PSO J236.2912+16.6088	15:45:09.90	+16:36:31.91	5.82	4	20.82	−25.89	1	1/1/1
SDSS J1545+6028	15:45:52.09	+60:28:23.95	5.78	4	19.04	−27.65	1	52/52/1
PSO J238.8510–06.8976	15:55:24.25	−06:53:51.59	5.81	4	20.65	−26.04	1	1/1/1
PSO J239.7124–07.4026	15:58:50.99	−07:24:09.59	6.11	4	19.32	−27.46	1	1/1/1
SDSS J1602+4228	16:02:53.98	+42:28:24.94	6.09	3	19.83	−26.94	1	5/22/1
ELAIS1091000446 [g]	16:03:49.07	+55:10:32.30	6.04	4	24.12	−22.64	0	44/44/44
ULAS J1609+3041	16:09:37.27	+30:41:47.78	6.14	3	20.41	−26.38	2	56/56/1
PSO J242.4397–12.9816	16:09:45.53	−12:58:54.11	5.83	4	19.78	−26.92	1	1/1/1
PSO J245.0636–00.1978	16:20:15.28	−00:11:52.30	5.68	4	21.39	−25.27	4	1/1/1
SDSS J1621+5155	16:21:00.92	+51:55:48.79	5.71	4	19.54	−27.13	0	17/17/1
SDSS J1623+3112	16:23:31.81	+31:12:00.53	6.26	1	20.26	−26.55	1	5/28/1
SDSS J1630+4012	16:30:33.90	+40:12:09.69	6.065	2	20.57	−26.19	1	4/22/1
CFHQS J1641+3755	16:41:21.73	+37:55:20.15	6.047	2	21.09	−25.67	1	15/25/1

Table 7
(Continued)

Quasar	R.A. (J2000)	Decl. (J2000)	z	Method [a]	m_{1450} [b] (mag)	M_{1450} (mag)	PS1 [c]	References disc./z/m_{1450}
PSO J267.0021+22.7812	17:48:00.51	+22:46:52.36	5.95	4	21.04	−25.70	1	1/1/1
PSO J293.0317+71.6523	19:32:07.62	+71:39:08.41	6.08	4	19.85	−26.92	1	1/1/1
PSO J308.0416–21.2339	20:32:09.99	−21:14:02.31	6.24	4	20.46	−26.35	2	1/1/1
PSO J308.4829–27.6485	20:33:55.91	−27:38:54.60	5.80	4	19.91	−26.78	1	1/1/1
SDSS J2053+0047	20:53:21.77	+00:47:06.80	5.92	4	21.44	−25.29	0	18/18/1
SDSS J2054–0005	20:54:06.49	−00:05:14.80	6.0391	1	20.55	−26.21	1	16/34/1
CFHQS J2100–1715	21:00:54.62	−17:15:22.50	6.087	2	21.22	−25.55	1	24/25/1
PSO J319.6040–10.9326	21:18:24.97	−10:55:57.43	5.90	4	20.00	−26.72	1	1/1/1
PSO J320.8703–24.3604	21:23:28.88	−24:21:37.44	5.73	4	20.46	−26.22	1	1/1/1
SDSS J2147+0107	21:47:55.41	+01:07:55.30	5.81	4	21.33	−25.37	0	18/18/1
PSO J328.7339–09.5076	21:54:56.16	−09:30:27.46	5.92	4	20.38	−26.34	1	1/1/1
IMS J2204+0012	22:04:17.92	+01:11:44.80	5.94	4	22.41	−24.32	0	45/45/1
PSO J333.9859+26.1081	22:15:56.63	+26:06:29.41	6.03	4	20.31	−26.44	2	1/1/1
HSC J2216–0016	22:16:44.47	−00:16:50.10	6.10	4	23.16	−23.62	0	53/53/53
VIMOS2911001793	22:19:17.22	+01:02:48.90	6.16	4	24.19	−22.60	0	44/44/1
SDSS J2220–0101	22:20:18.49	−01:01:46.89	5.62	4	20.66	−25.98	0	32/32/1
HSC J2228+0128 [f]	22:28:27.83	+01:28:09.50	6.01	4	24.34	−22.41	0	53/53/53
SDSS J2228+0110	22:28:43.54	+01:10:32.20	5.95	4	22.20	−24.54	0	29/29/29
CFHQS J2229+1457	22:29:01.65	+14:57:09.00	6.1517	1	22.01	−24.78	0	24/49/1
HSC J2232+0012 [f]	22:32:12.03	+00:12:38.40	6.18	4	24.04	−22.76	0	53/53/53
PSO J338.2298+29.5089	22:32:55.14	+29:30:32.31	6.658	2	20.78	−26.14	3	47/47/1
HSC J2236+0032 [e]	22:36:44.58	+00:32:56.90	6.40	4	23.25	−23.60	0	53/53/53
PSO J340.2041–18.6621	22:40:49.00	−18:39:43.81	6.01	4	20.34	−26.42	1	36/1/1
CFHQS J2242+0334	22:42:37.55	+03:34:21.60	5.88	4	22.20	−24.51	0	24/24/1
SDSS J2307+0031	23:07:35.35	+00:31:49.40	5.87	4	21.44	−25.27	0	18/18/1
SDSS J2310+1855	23:10:38.89	+18:55:19.93	6.0031	1	18.95	−27.80	2	34/34/1
SDSS J2315–0023	23:15:46.57	−00:23:58.10	6.12	4	21.12	−25.66	1	16/16/1
CFHQS J2318–0246	23:18:02.80	−02:46:34.00	6.05	4	21.66	−25.10	0	21/21/1
SDSS J2325+2628	23:25:14.24	+26:28:47.83	5.77	4	19.41	−27.27	1	52/52/1
CFHQS J2329–0301	23:29:08.28	−03:01:58.80	6.417	2	21.61	−25.25	0	15/25/1
CFHQS J2329–0403	23:29:14.46	−04:03:24.10	5.90	4	22.07	−24.65	0	21/21/1
VIK J2348–3054	23:48:33.34	−30:54:10.24	6.9018	1	21.17	−25.80	0	33/51/1
PSO J357.8289+06.4019	23:51:18.96	+06:24:06.92	5.81	4	21.41	−25.28	1	1/1/1
PSO J359.1352–06.3831	23:56:32.45	−06:22:59.26	6.15	4	20.00	−26.79	1	1;52/1/1
SDSS J2356+0023	23:56:51.58	+00:23:33.30	6.00	4	21.25	−25.50	0	18/18/1

Notes. Quasars sorted by right ascension. The reported coordinates are from PS1 when the quasars belong to the PS1 sample (PS1 column >0) or from their discovery papers otherwise.
[a] Method used to estimate the redshift: 1—[C II] or CO; 2—Mg II; 3—Other lines; 4—Template fitting or Lyα. The methods have typical redshift uncertainties smaller than 0.002, 0.015, 0.03, and 0.05, respectively. For details on individual quasars, we refer the reader to the redshift references.
[b] m_{1450} is calculated as in Section 4.2. The exceptions are VST-ATLAS J025.6821–33.4627, VST-ATLAS J029.9915–36.5658, ELAIS1091000446, and SDSS J2228+0110. These quasars do not have available y_{P1} or J magnitudes, and the m_{1450} from their discovery papers is reported.
[c] PS1 criteria: 0—None; 1—Criteria of Section 2.1.1 with $z_{P1} - y_{P1} < 0.5$; 2—Criteria of Section 2.1.1 with $z_{P1} - y_{P1} \geqslant 0.5$; 3—Criteria of Venemans et al. (2015a); 4—Extended PS1 criteria.
[d] CFHQS J0216–0455 (J0216–0455) could be a Seyfert galaxy (see Willott et al. 2009 and the appendix of Willott et al. 2010a).
[e] HSC J1205–0000 and HSC J2236+0032 have very uncertain redshifts (see Matsuoka et al. 2016).
[f] HSC J1207–0005, HSC J2228+0128, and HSC J2232+0012 are classified as "possible quasars," and they could be galaxies (see Matsuoka et al. 2016).
[g] ELAIS1091000446 (J1603+5510) could be a Lyα emitter (see Kashikawa et al. 2015).

References. (1) This work, (2) Fan et al. (2000), (3) Fan et al. (2001), (4) Fan et al. (2003), (5) Fan et al. (2004), (6) Mahabal et al. (2005), (7) Cool et al. (2006), (8) Fan et al. (2006), (9) Goto (2006), (10) McGreer et al. (2006), (11) Carilli et al. (2007), (12) Kurk et al. (2007), (13) Stern et al. (2007), (14) Venemans et al. (2007), (15) Willott et al. (2007), (16) Jiang et al. (2008), (17) Wang et al. (2008), (18) Jiang et al. (2009), (19) Kurk et al. (2009), (20) Mortlock et al. (2009), (21) Willott et al. (2009), (22) Carilli et al. (2010), (23) Wang et al. (2010), (24) Willott et al. (2010b), (25) Willott et al. (2010a), (26) De Rosa et al. (2011), (27) Mortlock et al. (2011), (28) Wang et al. (2011), (29) Zeimann et al. (2011), (30) Morganson et al. (2012), (31) Venemans et al. (2012), (32) McGreer et al. (2013), (33) Venemans et al. (2013), (34) Wang et al. (2013), (35) Willott et al. (2013), (36) Bañados et al. (2014), (37) Calura et al. (2014), (38) Leipski et al. (2014), (39) Bañados et al. (2015b), (40) Bañados et al. (2015a), (41) Becker et al. (2015b), (42) Carnall et al. (2015), (43) Jiang et al. (2015), (44) Kashikawa et al. (2015), (45) Kim et al. (2015), (46) Reed et al. (2015), (47) Venemans et al. (2015a), (48) Venemans et al. (2015b), (49) Willott et al. (2015), (50) Wu et al. (2015), (51) Venemans et al. (2016), (52) Wang et al. (2016a), (53) Matsuoka et al. (2016), (54) Wang et al. (2016b), (55) Jiang et al. (2016), (56) S. J. Warren et al. (2016, in preparation), (57) B. P. Venemans et al. (2016, in preparation).

(This table is available in its entirety in machine-readable form.)

Science Division of the NASA Science Mission Directorate); the National Science Foundation (under Grant No. AST-1238877); the University of Maryland; and Eotvos Lorand University.

This work is based on observations made with ESO Telescopes at the La Silla Paranal Observatory under programs 091.A-0421, 092.A-0150, 092.A-0339, 093.A-0574, 093.A-0863, 094.A-0053, 094.A-0079, 095.A-0375, 095.A-0535, 096.A-0291, 096.A-0420, 381.A-0486, and ID 179.A-2010 (PI. McMahon).

This paper includes data gathered with the 6.5 meter *Magellan* Telescopes located at Las Campanas Observatory,

Table 8
PS1, *J* Band, and *WISE* Photometry of the $z > 5.6$ Quasars Known as of 2016 March

Quasar	i_{P1} (mag)	z_{P1} (mag)	y_{P1} (mag)	*W*1 (mag)	*W*2 (mag)	*W*3 (mag)	*J* (mag)	J_{ref}	$E(B-V)$
P000+26	21.25 ± 0.04	19.28 ± 0.02	19.52 ± 0.04	19.07 ± 0.07	18.61 ± 0.11	⋯	19.53 ± 0.02	1	0.04
J0002+2550	21.82 ± 0.06	19.07 ± 0.01	19.40 ± 0.04	18.86 ± 0.06	18.88 ± 0.13	⋯	19.42 ± 0.09	2	0.04
J0005–0006	23.30 ± 0.24	20.44 ± 0.04	20.99 ± 0.16	20.00 ± 0.16	⋯	⋯	20.81 ± 0.10	7	0.03
P002–06	22.68 ± 0.13	20.25 ± 0.03	20.42 ± 0.10	19.51 ± 0.11	19.02 ± 0.14	⋯	19.86 ± 0.14	1	0.03
P002+32	>23.82	21.18 ± 0.06	21.15 ± 0.15	⋯	⋯	⋯	21.38 ± 0.19	1	0.04
P004+17	>23.31	20.82 ± 0.07	20.70 ± 0.13	20.71 ± 0.28	19.91 ± 0.32	⋯	20.67 ± 0.16	1	0.07
P004–24	22.31 ± 0.14	19.62 ± 0.02	19.43 ± 0.04	18.98 ± 0.07	18.91 ± 0.12	17.30 ± 0.34	19.30 ± 0.08	1	0.01
P007+04	22.84 ± 0.16	20.56 ± 0.05	20.12 ± 0.07	19.97 ± 0.16	19.75 ± 0.29	⋯	19.77 ± 0.11	20	0.01
J0033–0125	⋯	⋯	⋯	⋯	19.83 ± 0.29	⋯	21.58 ± 0.20	9	0.02
P009–08	21.98 ± 0.07	19.91 ± 0.03	20.16 ± 0.07	19.60 ± 0.11	19.69 ± 0.26	⋯	19.79 ± 0.08	1	0.04
P009–10	>23.79	20.82 ± 0.04	20.22 ± 0.07	19.22 ± 0.08	19.20 ± 0.16	⋯	19.93 ± 0.07	1	0.03
J0050+3445	>23.23	20.98 ± 0.07	20.14 ± 0.07	19.35 ± 0.07	19.13 ± 0.12	⋯	19.89 ± 0.04	15	0.08
J0055+0146	⋯	⋯	⋯	⋯	⋯	⋯	21.87 ± 0.15	14	0.02
J0100+2802	20.76 ± 0.04	18.61 ± 0.01	17.62 ± 0.01	17.16 ± 0.03	16.98 ± 0.03	16.89 ± 0.21	17.64 ± 0.02	2	0.06
J0102–0218	⋯	⋯	⋯	⋯	⋯	⋯	22.07 ± 0.17	14	0.04
J0109–3047	⋯	⋯	⋯	20.96 ± 0.32	⋯	⋯	21.27 ± 0.16	19	0.02
P021–25	22.17 ± 0.09	19.66 ± 0.03	19.62 ± 0.10	18.91 ± 0.06	18.83 ± 0.11	⋯	19.21 ± 0.05	1	0.02
J0129–0035	>23.75	22.17 ± 0.19	>21.67	⋯	⋯	⋯	22.72 ± 0.15	11	0.03
P023–02	22.98 ± 0.16	20.19 ± 0.03	20.28 ± 0.09	19.20 ± 0.07	18.82 ± 0.10	⋯	19.78 ± 0.10	1	0.03
J0136+0226	>23.70	22.06 ± 0.16	>21.83	⋯	⋯	⋯	22.09 ± 0.22	15	0.04
P025–11	22.72 ± 0.11	20.18 ± 0.03	19.85 ± 0.07	19.37 ± 0.08	19.26 ± 0.15	⋯	19.65 ± 0.06	1	0.02
J0142–3327	⋯	⋯	⋯	18.82 ± 0.05	18.82 ± 0.08	⋯	⋯	⋯	0.03
J0148+0600	22.50 ± 0.09	19.45 ± 0.01	19.37 ± 0.04	18.80 ± 0.06	18.61 ± 0.10	17.35 ± 0.29	19.30 ± 0.07	3	0.06
P029–29	22.03 ± 0.09	19.48 ± 0.02	19.44 ± 0.04	18.81 ± 0.05	18.58 ± 0.08	17.18 ± 0.29	19.07 ± 0.04	1	0.01
J0159–3633	⋯	⋯	⋯	19.39 ± 0.08	19.21 ± 0.12	⋯	⋯	⋯	0.01
J0203+0012	23.77 ± 0.27	20.74 ± 0.06	20.42 ± 0.09	19.39 ± 0.09	19.36 ± 0.19	⋯	19.99 ± 0.08	10	0.03
J0210–0456	⋯	⋯	⋯	⋯	⋯	⋯	22.28 ± 0.27	16	0.02
J0216–0455	⋯	⋯	⋯	⋯	⋯	⋯	24.20 ± 0.35	14	0.02
J0221–0802	⋯	⋯	⋯	20.69 ± 0.23	⋯	⋯	22.03 ± 0.14	15	0.03
P036+03	23.54 ± 0.24	21.44 ± 0.12	19.26 ± 0.03	19.43 ± 0.08	19.47 ± 0.18	⋯	19.51 ± 0.03	27	0.04
J0227–0605	⋯	⋯	⋯	20.85 ± 0.28	⋯	⋯	21.46 ± 0.16	14	0.03
P037–28	>23.65	20.73 ± 0.06	20.54 ± 0.12	20.19 ± 0.15	19.95 ± 0.26	⋯	20.41 ± 0.14	20	0.02
J0239–0045	⋯	⋯	⋯	⋯	⋯	⋯	21.15 ± 0.11	11	0.03
P040+17	23.09 ± 0.25	20.60 ± 0.05	20.85 ± 0.13	⋯	⋯	⋯	20.43 ± 0.10	1	0.09
P042–02	22.86 ± 0.15	20.49 ± 0.05	20.14 ± 0.06	20.28 ± 0.17	⋯	⋯	20.41 ± 0.10	1	0.05
P045–22	23.18 ± 0.20	20.34 ± 0.05	20.41 ± 0.14	⋯	⋯	⋯	19.65 ± 0.08	20	0.03
J0303–0019	>23.61	20.99 ± 0.06	21.23 ± 0.19	20.32 ± 0.12	20.17 ± 0.22	⋯	21.38 ± 0.08	12	0.11
J0305–3150	⋯	⋯	⋯	20.38 ± 0.14	20.09 ± 0.24	⋯	20.68 ± 0.07	19	0.01
J0316–1340	>23.63	21.57 ± 0.12	>21.69	⋯	⋯	⋯	21.77 ± 0.17	15	0.05
P049–26	>23.27	20.77 ± 0.06	20.92 ± 0.14	20.75 ± 0.18	⋯	⋯	⋯	⋯	0.02
J0328–3253	⋯	⋯	⋯	19.60 ± 0.07	19.53 ± 0.13	⋯	19.98 ± 0.03	28	0.01
P053–15	23.20 ± 0.27	20.34 ± 0.04	20.48 ± 0.12	⋯	⋯	⋯	⋯	⋯	0.09
P055–00	22.27 ± 0.13	20.19 ± 0.04	20.29 ± 0.09	20.62 ± 0.26	20.13 ± 0.35	⋯	20.10 ± 0.11	4	0.09
P056–16	22.99 ± 0.28	20.00 ± 0.04	20.05 ± 0.08	19.50 ± 0.09	19.20 ± 0.14	⋯	20.25 ± 0.10	1	0.05
J0353+0104	>23.21	20.81 ± 0.07	20.36 ± 0.13	19.34 ± 0.09	19.62 ± 0.24	⋯	20.38 ± 0.11	4	0.28
P060+24	23.01 ± 0.30	20.18 ± 0.03	19.87 ± 0.06	19.17 ± 0.09	19.41 ± 0.21	⋯	19.71 ± 0.05	1	0.23
P065–26	22.65 ± 0.18	20.48 ± 0.05	19.56 ± 0.05	19.01 ± 0.06	19.00 ± 0.10	⋯	19.32 ± 0.06	1	0.04
P065–19	23.47 ± 0.24	19.79 ± 0.03	20.19 ± 0.08	18.67 ± 0.05	18.42 ± 0.07	17.24 ± 0.31	19.90 ± 0.15	1	0.04
P071–04	22.47 ± 0.11	20.30 ± 0.04	20.13 ± 0.08	⋯	⋯	⋯	20.27 ± 0.07	1	0.04
P071–02	21.25 ± 0.05	19.18 ± 0.01	19.14 ± 0.03	18.95 ± 0.06	18.90 ± 0.11	⋯	19.02 ± 0.03	1	0.04
J0454–4448	⋯	⋯	⋯	19.68 ± 0.08	19.62 ± 0.14	⋯	20.24 ± 0.07	26	0.01
P075–07	>23.40	20.33 ± 0.05	20.11 ± 0.08	19.70 ± 0.11	19.58 ± 0.20	17.02 ± 0.32	20.52 ± 0.12	1	0.19
P089–15	>23.17	19.66 ± 0.03	19.85 ± 0.09	18.22 ± 0.04	17.88 ± 0.05	17.24 ± 0.28	19.17 ± 0.04	1	0.30
P108+08	22.69 ± 0.22	19.45 ± 0.02	19.15 ± 0.03	18.69 ± 0.06	18.51 ± 0.09	⋯	19.29 ± 0.06	1	0.09
J0810+5105	22.29 ± 0.10	19.70 ± 0.02	19.89 ± 0.06	19.64 ± 0.10	19.20 ± 0.14	⋯	⋯	⋯	0.05
J0818+1722	22.26 ± 0.08	19.55 ± 0.02	19.26 ± 0.03	18.70 ± 0.03	18.36 ± 0.05	⋯	19.48 ± 0.05	7	0.04
J0828+2633	>23.44	20.72 ± 0.06	20.42 ± 0.10	19.33 ± 0.06	19.39 ± 0.13	⋯	20.41 ± 0.13	3	0.08
P127+03	>23.13	20.69 ± 0.05	20.69 ± 0.11	20.07 ± 0.17	19.87 ± 0.28	⋯	20.80 ± 0.21	1	0.04
J0836+0054	20.99 ± 0.04	18.70 ± 0.01	18.96 ± 0.02	18.00 ± 0.04	17.75 ± 0.05	⋯	18.64 ± 0.03	3	0.05
J0839+0015	>23.59	21.18 ± 0.09	>21.68	20.15 ± 0.18	⋯	⋯	20.89 ± 0.11	28	0.04
J0840+5624	21.97 ± 0.07	19.75 ± 0.02	19.47 ± 0.05	19.46 ± 0.14	19.30 ± 0.22	⋯	19.94 ± 0.10	7	0.04
J0841+2905	>23.00	20.33 ± 0.05	20.26 ± 0.08	19.91 ± 0.16	19.60 ± 0.25	⋯	20.02 ± 0.09	3	0.05
J0842+1218	>23.43	19.83 ± 0.03	19.88 ± 0.06	18.92 ± 0.07	19.31 ± 0.18	⋯	19.78 ± 0.03	23	0.07

Table 8
(Continued)

Quasar	i_{P1} (mag)	z_{P1} (mag)	y_{P1} (mag)	$W1$ (mag)	$W2$ (mag)	$W3$ (mag)	J (mag)	J_{ref}	$E(B-V)$
J0850+3246	22.48 ± 0.15	20.17 ± 0.03	20.00 ± 0.05	19.43 ± 0.09	18.98 ± 0.15	⋯	19.69 ± 0.08	2	0.03
J0859+0022	⋯	⋯	⋯	⋯	⋯	⋯	>22.32	29	0.03
P135+16	22.45 ± 0.15	20.67 ± 0.04	20.74 ± 0.12	19.51 ± 0.11	19.53 ± 0.22	⋯	20.30 ± 0.12	21	0.04
P135–13	22.66 ± 0.19	20.31 ± 0.04	20.87 ± 0.12	⋯	⋯	⋯	20.80 ± 0.14	1	0.07
J0927+2001	21.92 ± 0.10	19.88 ± 0.02	19.93 ± 0.08	19.40 ± 0.11	⋯	⋯	19.95 ± 0.10	7	0.03
J1030+0524	23.54 ± 0.28	20.19 ± 0.04	19.90 ± 0.06	19.28 ± 0.09	18.91 ± 0.15	⋯	19.79 ± 0.08	3	0.02
P157–02	22.72 ± 0.18	20.24 ± 0.03	20.29 ± 0.07	19.54 ± 0.11	19.54 ± 0.22	⋯	20.20 ± 0.10	1	0.05
P159–02	>23.62	20.46 ± 0.04	19.88 ± 0.06	19.44 ± 0.09	19.04 ± 0.13	⋯	20.00 ± 0.10	1	0.05
J1044–0125	21.62 ± 0.08	19.31 ± 0.01	19.31 ± 0.03	19.05 ± 0.07	18.97 ± 0.14	⋯	19.25 ± 0.05	3	0.05
J1048+4637	22.54 ± 0.10	20.07 ± 0.03	19.59 ± 0.06	19.05 ± 0.06	19.20 ± 0.12	⋯	19.31 ± 0.05	6	0.02
J1059–0906	>23.82	20.84 ± 0.06	21.50 ± 0.34	20.08 ± 0.17	19.75 ± 0.25	⋯	20.79 ± 0.07	15	0.03
P167+56	23.72 ± 0.32	20.84 ± 0.06	20.75 ± 0.14	⋯	⋯	⋯	20.31 ± 0.14	1	0.01
P167–13	>23.45	>22.86	20.48 ± 0.11	⋯	⋯	⋯	21.21 ± 0.09	27	0.06
J1120+0641	⋯	⋯	⋯	19.61 ± 0.11	19.42 ± 0.20	⋯	20.36 ± 0.05	1	0.05
P172+26	23.42 ± 0.30	20.80 ± 0.05	20.79 ± 0.11	19.88 ± 0.14	20.04 ± 0.31	⋯	20.44 ± 0.14	1	0.02
J1137+3549	22.23 ± 0.08	19.46 ± 0.01	19.42 ± 0.03	19.16 ± 0.07	19.23 ± 0.14	⋯	19.35 ± 0.05	7	0.02
P174–12	23.11 ± 0.32	20.04 ± 0.04	20.21 ± 0.10	19.72 ± 0.12	19.25 ± 0.16	⋯	20.34 ± 0.19	4	0.03
P175–20	22.56 ± 0.20	20.17 ± 0.04	20.35 ± 0.08	19.17 ± 0.08	19.68 ± 0.25	⋯	19.96 ± 0.13	4	0.05
J1143+3808	22.43 ± 0.08	20.11 ± 0.03	20.02 ± 0.05	19.63 ± 0.10	19.37 ± 0.16	⋯	19.95 ± 0.14	2	0.02
J1148+0702	23.28 ± 0.26	20.99 ± 0.07	20.37 ± 0.11	19.09 ± 0.08	18.82 ± 0.13	⋯	20.30 ± 0.11	3	0.02
J1148+5253	⋯	⋯	⋯	⋯	⋯	⋯	22.39 ± 0.06	6	0.02
J1148+5251	22.71 ± 0.12	20.56 ± 0.03	19.01 ± 0.04	18.67 ± 0.05	18.79 ± 0.08	⋯	19.19 ± 0.05	6	0.02
J1148+0056	>23.49	21.75 ± 0.10	21.35 ± 0.19	21.28 ± 0.33	⋯	⋯	21.79 ± 0.10	28	0.03
J1152+0055	⋯	⋯	⋯	⋯	⋯	⋯	21.66 ± 0.22	29	0.02
P178–12	>23.36	20.86 ± 0.08	20.61 ± 0.11	20.44 ± 0.23	⋯	⋯	20.78 ± 0.09	1	0.05
J1202–0057	⋯	⋯	⋯	⋯	⋯	⋯	>22.32	29	0.03
J1205–0000	⋯	⋯	⋯	19.98 ± 0.15	19.65 ± 0.23	⋯	21.95 ± 0.21	29	0.02
J1207+0630	22.98 ± 0.17	20.44 ± 0.03	20.15 ± 0.07	19.69 ± 0.13	19.43 ± 0.21	⋯	20.29 ± 0.14	3	0.02
J1207–0005	⋯	⋯	⋯	⋯	⋯	⋯	>22.32	29	0.02
P183–12	22.14 ± 0.13	19.47 ± 0.02	19.23 ± 0.03	18.98 ± 0.07	19.18 ± 0.16	⋯	19.10 ± 0.04	4	0.05
J1215+0023	>23.88	21.35 ± 0.10	21.29 ± 0.15	⋯	⋯	⋯	21.32 ± 0.14	28	0.02
P184+01	>23.74	21.20 ± 0.07	21.46 ± 0.20	20.28 ± 0.21	⋯	⋯	⋯	⋯	0.02
P187–02	>23.74	20.92 ± 0.05	20.88 ± 0.10	19.89 ± 0.14	19.97 ± 0.32	⋯	20.73 ± 0.13	1	0.03
P187+04	23.44 ± 0.26	20.92 ± 0.04	21.11 ± 0.13	21.00 ± 0.30	⋯	⋯	⋯	⋯	0.02
J1243+2529	23.43 ± 0.26	20.24 ± 0.03	20.63 ± 0.08	19.40 ± 0.09	18.86 ± 0.11	⋯	20.14 ± 0.12	3	0.02
J1250+3130	23.12 ± 0.19	19.88 ± 0.02	20.28 ± 0.08	19.11 ± 0.07	18.71 ± 0.09	⋯	19.86 ± 0.11	3	0.01
P194+25	23.28 ± 0.21	20.60 ± 0.04	20.91 ± 0.15	20.00 ± 0.08	19.72 ± 0.14	⋯	⋯	⋯	0.01
J1257+6349	22.85 ± 0.21	20.80 ± 0.07	20.50 ± 0.14	19.61 ± 0.08	19.86 ± 0.19	⋯	20.72 ± 0.08	23	0.01
J1306+0356	22.50 ± 0.19	19.76 ± 0.03	19.96 ± 0.06	19.57 ± 0.10	⋯	⋯	19.71 ± 0.10	5	0.03
P197+25	23.66 ± 0.31	20.95 ± 0.06	20.71 ± 0.12	20.28 ± 0.17	⋯	⋯	⋯	⋯	0.01
J1319+0950	22.86 ± 0.15	20.13 ± 0.02	19.76 ± 0.04	19.73 ± 0.11	19.65 ± 0.21	⋯	19.70 ± 0.03	13	0.02
P201+57	23.21 ± 0.29	20.43 ± 0.05	20.63 ± 0.15	20.07 ± 0.12	19.54 ± 0.16	⋯	20.16 ± 0.24	1	0.01
J1335+3533	22.87 ± 0.16	20.22 ± 0.02	20.06 ± 0.06	19.41 ± 0.07	19.33 ± 0.13	⋯	19.91 ± 0.05	7	0.01
P209–26	21.68 ± 0.09	19.35 ± 0.01	19.49 ± 0.04	19.07 ± 0.08	19.08 ± 0.15	17.11 ± 0.21	19.35 ± 0.05	1	0.06
P210+27	>23.75	21.18 ± 0.06	20.27 ± 0.08	20.26 ± 0.16	20.32 ± 0.35	⋯	20.35 ± 0.15	3	0.02
P210+40	>23.86	20.87 ± 0.05	20.92 ± 0.12	⋯	⋯	⋯	⋯	⋯	0.02
P210+09	23.02 ± 0.16	20.31 ± 0.03	20.31 ± 0.09	19.98 ± 0.12	20.09 ± 0.29	⋯	21.03 ± 0.23	1	0.03
P210–12	>23.21	21.09 ± 0.07	20.89 ± 0.13	⋯	19.93 ± 0.29	⋯	20.47 ± 0.20	4	0.07
P212–15	>23.44	20.98 ± 0.06	21.27 ± 0.19	⋯	⋯	⋯	20.63 ± 0.15	1	0.10
J1411+1217	23.33 ± 0.25	19.58 ± 0.02	20.05 ± 0.08	19.29 ± 0.07	18.87 ± 0.09	⋯	19.89 ± 0.05	7	0.02
P213–22	22.68 ± 0.22	19.55 ± 0.02	19.89 ± 0.08	19.46 ± 0.17	18.97 ± 0.19	⋯	⋯	⋯	0.09
P213–13	>23.58	20.86 ± 0.05	21.01 ± 0.20	⋯	⋯	⋯	⋯	⋯	0.08
P215–16	21.48 ± 0.05	19.08 ± 0.02	19.14 ± 0.03	18.27 ± 0.05	18.12 ± 0.07	16.96 ± 0.20	18.86 ± 0.03	4	0.08
J1425+3254	22.89 ± 0.17	20.41 ± 0.03	20.26 ± 0.07	19.67 ± 0.08	19.66 ± 0.16	⋯	20.37 ± 0.17	2	0.01
J1427+3312	⋯	⋯	⋯	19.52 ± 0.08	19.26 ± 0.12	⋯	20.62 ± 0.05	8	0.01
P217–16	23.18 ± 0.29	20.46 ± 0.04	19.87 ± 0.06	18.99 ± 0.08	19.39 ± 0.18	⋯	19.69 ± 0.07	1	0.09
J1429+5447	23.52 ± 0.31	21.87 ± 0.14	20.88 ± 0.16	19.73 ± 0.08	20.49 ± 0.32	⋯	20.64 ± 0.07	15	0.02
P217–07	>23.79	21.10 ± 0.08	20.44 ± 0.08	19.88 ± 0.12	19.81 ± 0.25	⋯	19.87 ± 0.07	4	0.07
J1436+5007	22.65 ± 0.16	20.03 ± 0.03	20.16 ± 0.06	19.87 ± 0.09	20.30 ± 0.25	⋯	19.98 ± 0.10	7	0.02
J1509–1749	>22.68	20.04 ± 0.03	19.66 ± 0.06	⋯	⋯	⋯	19.82 ± 0.08	4	0.09
P228+21	>23.97	20.92 ± 0.06	20.63 ± 0.10	20.57 ± 0.12	20.30 ± 0.21	⋯	20.89 ± 0.18	1	0.05
P235+17	22.57 ± 0.12	20.23 ± 0.03	20.18 ± 0.07	19.49 ± 0.08	19.85 ± 0.24	17.52 ± 0.31	19.92 ± 0.08	1	0.03
P236+16	23.45 ± 0.24	20.69 ± 0.05	20.82 ± 0.11	20.41 ± 0.13	19.90 ± 0.17	⋯	20.73 ± 0.12	1	0.03

Table 8
(Continued)

Quasar	i_{P1} (mag)	z_{P1} (mag)	y_{P1} (mag)	$W1$ (mag)	$W2$ (mag)	$W3$ (mag)	J (mag)	J_{ref}	$E(B-V)$
J1545+6028	21.42 ± 0.06	18.82 ± 0.01	19.04 ± 0.04	18.71 ± 0.04	18.50 ± 0.05	17.49 ± 0.23	⋯	⋯	0.01
P238–06	23.12 ± 0.27	20.43 ± 0.05	20.66 ± 0.12	⋯	⋯	⋯	20.11 ± 0.12	1	0.17
P239–07	22.93 ± 0.24	19.78 ± 0.03	19.34 ± 0.04	⋯	⋯	⋯	19.35 ± 0.11	4	0.17
J1602+4228	22.83 ± 0.13	20.12 ± 0.03	19.85 ± 0.05	18.75 ± 0.04	18.46 ± 0.06	17.54 ± 0.26	19.40 ± 0.05	7	0.01
J1603+5510	⋯	⋯	⋯	⋯	⋯	⋯	>24.69	24	0.01
J1609+3041	23.55 ± 0.27	20.98 ± 0.07	20.43 ± 0.09	20.22 ± 0.14	20.42 ± 0.35	⋯	20.62 ± 0.15	3	0.03
P242–12	22.69 ± 0.21	19.76 ± 0.04	19.79 ± 0.10	19.00 ± 0.07	19.44 ± 0.23	17.04 ± 0.32	19.59 ± 0.08	1	0.30
P245–00	23.66 ± 0.28	21.15 ± 0.07	21.39 ± 0.24	21.14 ± 0.27	⋯	⋯	21.10 ± 0.19	1	0.10
J1621+5155	21.89 ± 0.06	20.04 ± 0.04	19.86 ± 0.05	18.35 ± 0.03	18.11 ± 0.04	18.06 ± 0.32	19.46 ± 0.10	2	0.02
J1623+3112	23.27 ± 0.26	20.04 ± 0.04	20.29 ± 0.10	19.22 ± 0.06	19.00 ± 0.10	⋯	20.09 ± 0.10	7	0.02
J1630+4012	22.92 ± 0.14	20.47 ± 0.04	20.59 ± 0.11	20.19 ± 0.12	⋯	⋯	20.32 ± 0.10	6	0.01
J1641+3755	>24.02	21.35 ± 0.07	21.11 ± 0.17	⋯	⋯	⋯	21.24 ± 0.14	9	0.02
P267+22	>23.65	20.89 ± 0.06	21.05 ± 0.13	⋯	⋯	⋯	21.02 ± 0.22	1	0.10
P293+71	>23.25	19.66 ± 0.04	19.88 ± 0.11	20.07 ± 0.08	19.82 ± 0.12	⋯	19.67 ± 0.05	1	0.17
P308–21	23.58 ± 0.27	21.12 ± 0.08	20.49 ± 0.11	19.20 ± 0.09	18.78 ± 0.13	⋯	20.17 ± 0.11	1	0.05
P308–27	22.31 ± 0.10	19.71 ± 0.02	19.92 ± 0.08	19.63 ± 0.12	19.37 ± 0.22	⋯	19.46 ± 0.06	1	0.05
J2053+0047	>23.83	21.59 ± 0.13	21.78 ± 0.31	20.82 ± 0.32	⋯	⋯	21.37 ± 0.07	11	0.08
J2054–0005	23.49 ± 0.29	21.03 ± 0.09	20.57 ± 0.13	⋯	⋯	⋯	20.59 ± 0.15	4	0.10
J2100–1715	23.97 ± 0.35	21.55 ± 0.09	21.24 ± 0.21	⋯	⋯	⋯	21.42 ± 0.10	15	0.07
P319–10	23.22 ± 0.20	19.94 ± 0.02	20.02 ± 0.06	18.84 ± 0.07	18.58 ± 0.11	⋯	20.02 ± 0.05	1	0.05
P320–24	23.01 ± 0.21	20.17 ± 0.04	20.46 ± 0.15	19.85 ± 0.15	19.82 ± 0.34	⋯	20.26 ± 0.10	1	0.04
J2147+0107	>23.73	21.39 ± 0.09	>21.34	20.33 ± 0.20	⋯	⋯	21.73 ± 0.14	11	0.12
P328–09	23.21 ± 0.15	20.82 ± 0.06	20.40 ± 0.11	20.43 ± 0.24	⋯	⋯	20.26 ± 0.16	4	0.04
J2204+0112	⋯	⋯	⋯	⋯	⋯	⋯	22.34 ± 0.08	25	0.05
P333+26	>23.53	20.91 ± 0.09	20.33 ± 0.10	20.88 ± 0.20	20.13 ± 0.21	⋯	20.44 ± 0.05	1	0.11
J2216–0016	⋯	⋯	⋯	⋯	⋯	⋯	⋯	⋯	0.07
J2219+0102	⋯	⋯	⋯	⋯	⋯	⋯	24.13 ± 0.31	24	0.08
J2220–0101	21.74 ± 0.07	20.36 ± 0.05	20.66 ± 0.12	19.84 ± 0.09	19.56 ± 0.14	⋯	20.42 ± 0.19	18	0.07
J2228+0128	⋯	⋯	⋯	⋯	⋯	⋯	⋯	⋯	0.07
J2228+0110	⋯	⋯	⋯	⋯	⋯	⋯	>20.90	17	0.07
J2229+1457	>23.97	21.84 ± 0.12	>21.99	21.34 ± 0.31	⋯	⋯	21.95 ± 0.07	15	0.06
J2232+0012	⋯	⋯	⋯	⋯	⋯	⋯	⋯	⋯	0.07
P338+29	>23.29	>22.50	20.23 ± 0.10	20.51 ± 0.21	⋯	⋯	20.74 ± 0.09	27	0.10
J2236+0032	⋯	⋯	⋯	⋯	⋯	⋯	⋯	⋯	0.07
P340–18	23.34 ± 0.29	20.14 ± 0.03	20.35 ± 0.10	19.26 ± 0.09	18.87 ± 0.13	⋯	20.28 ± 0.08	20	0.03
J2242+0334	⋯	⋯	⋯	⋯	⋯	⋯	22.13 ± 0.12	15	0.08
J2307+0031	>23.89	21.71 ± 0.12	21.67 ± 0.25	19.78 ± 0.13	19.61 ± 0.25	⋯	21.37 ± 0.11	11	0.05
J2310+1855	21.53 ± 0.08	19.50 ± 0.03	18.97 ± 0.03	18.50 ± 0.05	18.75 ± 0.12	⋯	18.88 ± 0.05	2	0.17
J2315–0023	>23.71	20.97 ± 0.06	21.14 ± 0.16	20.26 ± 0.20	⋯	⋯	20.88 ± 0.08	10	0.04
J2318–0246	>23.47	22.09 ± 0.17	>21.82	⋯	⋯	⋯	21.60 ± 0.11	14	0.04
J2325+2628	21.94 ± 0.09	19.61 ± 0.02	19.42 ± 0.04	18.89 ± 0.06	18.75 ± 0.10	⋯	18.91 ± 0.03	1	0.10
J2329–0301	>23.74	22.10 ± 0.21	21.79 ± 0.33	⋯	⋯	⋯	21.56 ± 0.25	9	0.05
J2329–0403	>23.50	21.29 ± 0.11	>21.91	⋯	⋯	⋯	22.00 ± 0.19	14	0.05
J2348–3054	⋯	⋯	⋯	20.37 ± 0.17	⋯	⋯	21.14 ± 0.08	19	0.01
P357+06	>24.19	21.31 ± 0.10	21.42 ± 0.21	⋯	⋯	⋯	21.69 ± 0.35	1	0.08
P359–06	23.02 ± 0.21	19.97 ± 0.03	20.03 ± 0.06	19.26 ± 0.10	19.04 ± 0.19	⋯	19.85 ± 0.10	1	0.03
J2356+0023	>24.16	22.15 ± 0.22	21.41 ± 0.28	⋯	⋯	⋯	21.18 ± 0.07	11	0.04

Notes. Quasars sorted by right ascension; their full names, coordinates, and redshifts are given in Table 7. The PS1 magnitudes are *dereddened*. Reddened magnitudes can be obtained by adding $\lambda_f \times E(B-V)$ with $\lambda_f = (1.682, 1.322, 1.087)$ for (i_{P1}, z_{P1}, y_{P1}); see Schlafly and Finkbeiner (2011). *WISE* magnitudes are reported when their measurements have S/N < 3. They are from the ALLWISE source catalog when available. The magnitudes of J0033–0125, J0109–3040, J0221–0802, J0227–0605, P055–00, P167–13, P210–12, J1641+3755, J2053+0047, and P328–09 were taken from the ALLWISE reject table. The magnitudes of P209–26, P215–16, and P217–16 were taken from the *WISE* All-Sky data release catalog. The UKIRT Hemisphere Survey (UHS) (http://casu.ast.cam.ac.uk/wfcamsp/uhs) was not used for our selection, but here we provide the *J* band photometry for known quasars detected in the catalog.

References. (1) This work, (2) UHS, (3) UKIDSS, (4) VHS, (5) Fan et al. (2001), (6) Fan et al. (2003), (7) Fan et al. (2004), (8) McGreer et al. (2006), (9) Willott et al. (2007), (10) Jiang et al. (2008), (11) Jiang et al. (2009), (12) Kurk et al. (2009), (13) Mortlock et al. (2009), (14) Willott et al. (2009), (15) Willott et al. (2010b), (16) Willott et al. (2010a), (17) Zeimann et al. (2011), (18) McGreer et al. (2013), (19) Venemans et al. (2013), (20) Bañados et al. (2014), (21) Bañados et al. (2015b), (22) Barnett et al. (2015), (23) Jiang et al. (2015), (24) Kashikawa et al. (2015), (25) Kim et al. (2015), (26) Reed et al. (2015), (27) Venemans et al. (2015a), (28) Venemans et al. (2015b), (29) Matsuoka et al. (2016).

(This table is available in its entirety in machine-readable form.)

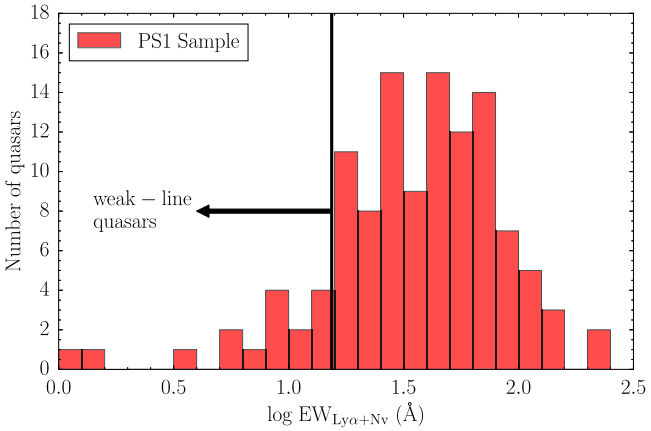

Figure 11. Distribution of rest-frame EW(Lyα + N v) for 117 $z > 5.6$ quasars from the PS1 sample (see Section 7). According to the definition of weak-line quasars at EW(Lyα + N v) < 15.4 Å (Diamond-Stanic et al. 2009), 13.7% (16/117) of the PS1 quasars fall in this category.

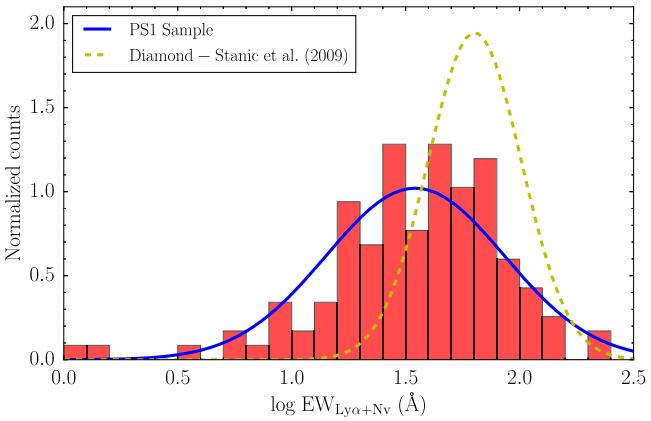

Figure 12. Normalized counts of the EW(Lyα + N v) distribution from Figure 11. The blue line shows the log-normal distribution best fit to the data, with $\langle \log \mathrm{EW}\ (\text{Å}) \rangle = 1.542$ and $\sigma(\log \mathrm{EW}\ (\text{Å})) = 0.391$. The dashed yellow line is the best-fit distribution found at lower redshift by Diamond-Stanic et al. (2009), with $\langle \log \mathrm{EW}\ (\text{Å}) \rangle = 1.803$ and $\sigma(\log \mathrm{EW}\ (\text{Å})) = 0.205$. The PS1 sample distribution is systematically shifted to smaller EWs and has a larger dispersion. This could be due to the stronger IGM absorption at $z > 5.6$. Alternatively, this might be an indication of a change of the EW distribution with redshift.

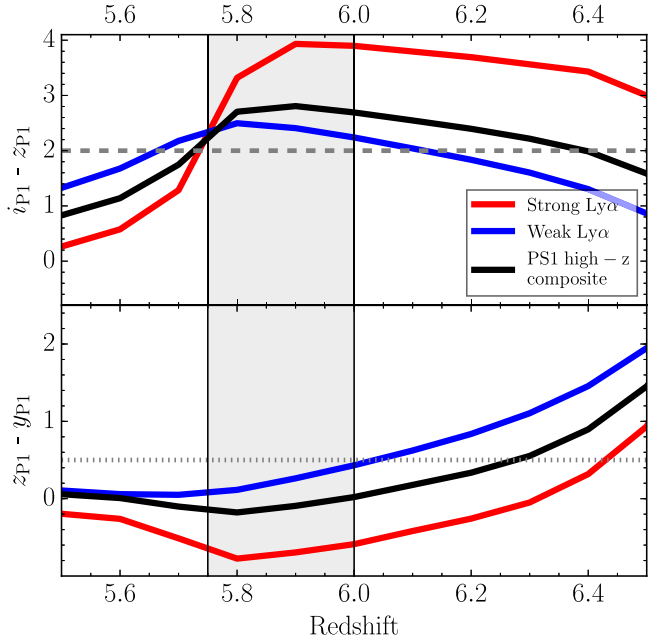

Figure 13. Redshift vs. $i_{P1} - z_{P1}$ (top) and $z_{P1} - y_{P1}$ (bottom) colors. The red, blue, and black solid lines are the color tracks of the composite spectra from Section 6 (see legend and Figure 10) redshifted from $z = 5.5$ to $z = 6.5$. The gray dashed line shows our selection criteria $i_{P1} - z_{P1} > 2$, while the dotted line at $z_{P1} - y_{P1} = 0.5$ shows the boundary for which we have different selection criteria (Section 2.1.1). Quasars with a weak Lyα line at $z > 6.2$ are difficult to identify with our current color selection. The shaded area at $5.75 < z < 6.00$ represents the region where we are sensitive to selecting quasars with both strong and weak Lyα emission lines.

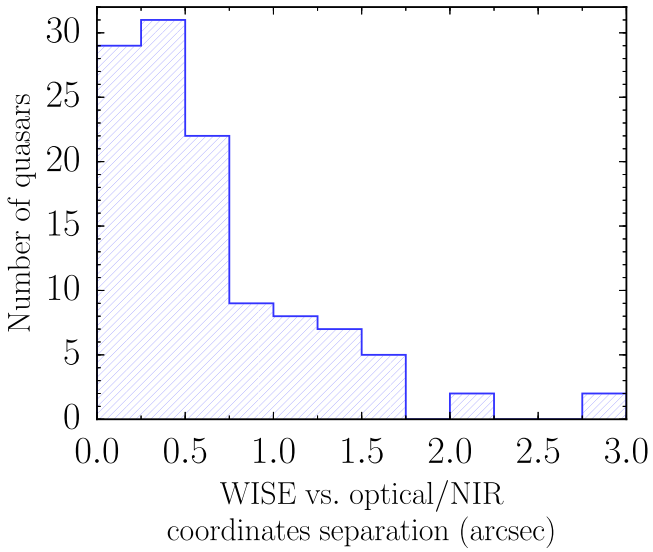

Figure 14. Separation in arcsec between the *WISE* and optical/near-infrared coordinates of the known $z > 5.6$ quasars with at least a 3σ detection in one of the *WISE* bands. The four quasars with a separation greater than 2″ are P135 +16, P187–02, P242–12, and P197+25.

Chile. The FIRE observations were supported by the NSF under grant AST-1109915.

Some of the data presented herein were obtained at the W. M. Keck Observatory, which is operated as a scientific partnership between the California Institute of Technology, the University of California, and the National Aeronautics and Space Administration. The observatory was made possible by the generous financial support of the W. M. Keck Foundation. The authors wish to recognize the very significant cultural role that the summit of Mauna Kea has always had within the indigenous Hawaiian community, who hold this feature in deep reverence. We are most fortunate to have the opportunity to conduct observations from this mountain.

Part of our data is based on observations collected at the Centro Astronómico Hispano Alemán at Calar Alto, jointly operated by the Max-Planck Institut für Astronomie and the Instituto de Astrofísica de Andalucía.

Some of the observations reported here were obtained at the MMT Observatory, a joint facility of the University of Arizona and the Smithsonian Institution.

The LBT is an international collaboration among institutions in the United States, Italy, and Germany. The LBT Corporation partners are the University of Arizona, on behalf of the Arizona University System; Istituto Nazionale di Astrofisica, Italy; LBT Beteiligungsgesellschaft, Germany, representing the Max

Planck Society, the Astrophysical Institute Potsdam, and Heidelberg University; the Ohio State University; and Research Corporation, on behalf of the University of Notre Dame, the University of Minnesota, and the University of Virginia. This paper used data obtained with the MODS spectrograph, built with funding from NSF grant AST-9987045 and the NSF Telescope System Instrumentation Program and with additional funds from the Ohio Board of Regents and the Ohio State University Office of Research.

Part of the funding for GROND (both hardware and personnel) was generously granted from the Leibniz Prize to Prof. G. Hasinger (DFG grant HA 1850/28-1).

UKIDSS and UHS use the UKIRT Wide Field Camera (Casali et al. 2007) and the photometric system described in Hewett et al. (2006). The science archive is described in Hambly et al. (2008).

This publication makes use of data products from the *Wide-Field Infrared Survey Explorer*, which is a joint project of the University of California, Los Angeles, and the Jet Propulsion Laboratory/California Institute of Technology, funded by the National Aeronautics and Space Administration.

This research has benefitted from the SpeX Prism Spectral Libraries, maintained by Adam Burgasser at http://pono.ucsd.edu/~adam/browndwarfs/spexprism.

This research made use of Astropy, a community-developed core Python package for astronomy (Astropy Collaboration et al. 2013, http://www.astropy.org). The plots in this publication were produced using Matplotlib (Hunter 2007, http://www.matplotlib.org).

Facilities: PS1 (GPC1), VLT:Antu (FORS2), NTT (EFOSC2), LBT (MODS), Max Planck:2.2m (GROND), Magellan:Baade (FIRE), Magellan:Clay (LDSS3), Keck:I (LRIS), Hale (DBSP), CAO:3.5 m (Omega2000), CAO:2.2 m (CAFOS), MMT (SWIRC), Du Pont (Retrocam).

APPENDIX A
LIST OF QUASARS AT $z > 5.6$

Table 7 lists the full names, coordinates, redshifts, and rest-frame 1450 Å magnitudes for the 173 $z > 5.6$ quasars known as of the end of 2016 March. The table column "PS1" is >0 for quasars that satisfy the selection criteria presented in Section 2 and Venemans et al. (2015a). There are 124 PS1-selected quasars, of which 77 are PS1 discoveries.

APPENDIX B
PAN-STARRS1, *J*, AND *WISE* PHOTOMETRY OF THE KNOWN $z > 5.6$ QUASARS

The quasars were cross-matched to the *WISE* All-Sky data release product catalog (Cutri 2012) and to the ALLWISE Source catalog and Reject Table[23] (Cutri 2014) within a radius of 3″ (note that the *WISE* PSF FWHM for *W*1 and *W*2 is about 6″). Figure 14 shows a histogram with the separation between the optical/near-infrared and *WISE* positions. Most of the *WISE* coordinates are within 2″ from the optical/near-infrared locations. The four objects with a separation greater than 2″ are P135+16, P187–02, P242–12, and P197+25, with separations of 2.″95, 2.″83, 2.″11, and 2.″02, respectively. Therefore, their *WISE* magnitudes must be used with caution. As a test we can compare the *W*1 magnitudes of three of these objects with their

[23] http://wise2.ipac.caltech.edu/docs/release/allwise/expsup/sec2_1.html

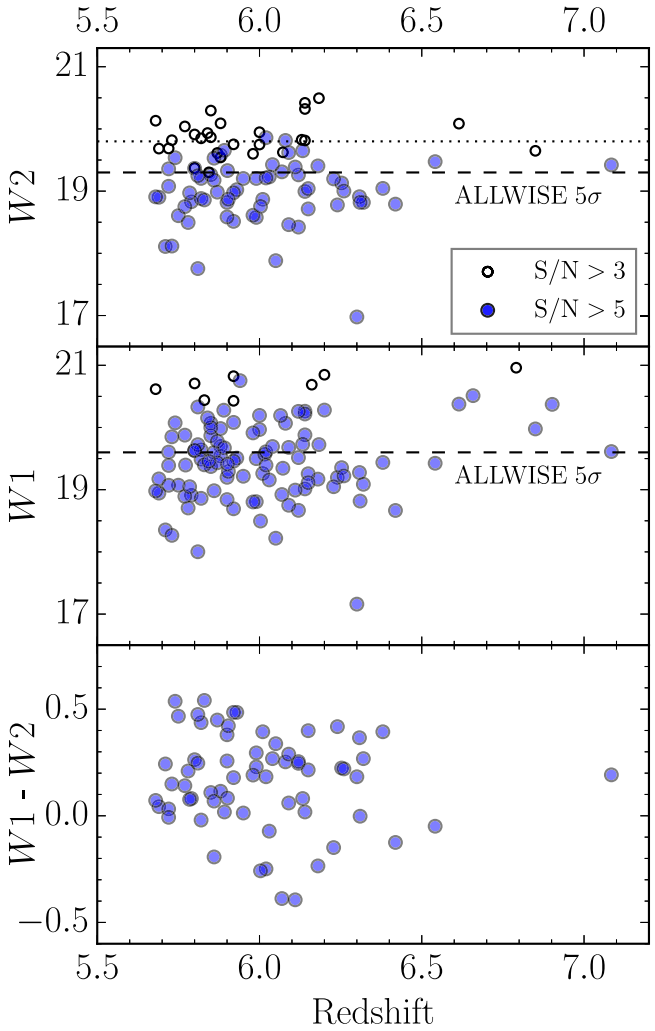

Figure 15. *WISE* *W*1 (middle) and *W*2 (top) magnitudes vs. redshift for all $z > 5.6$ quasars detected in at least one of the *WISE* bands with S/N > 3. The bottom panel shows the $W1 - W2$ color vs. redshift for quasars with S/N > 5 in both bands. The dashed lines represent the nominal ALLWISE 5σ limiting magnitudes, while the dotted line on the top panel represents the expected median limiting magnitude once ALLWISE is combined with the ongoing NEOWISE reactivated program.

Spitzer 3.6 μm photometry, taken with our *Spitzer* survey of our PS1 quasar sample (Program: 11030; PI: R. Decarli; details of the survey will be presented by R. Decarli 2016, in preparation). The *W*1 magnitudes for P135+16, P187–02, and P242–12 are 19.51 ± 0.11, 19.89 ± 0.14, and 19.00 ± 0.07, while their *Spitzer* 3.6 μm magnitudes are 20.49 ± 0.02, 20.38 ± 0.01, and 19.30 ± 0.01. The magnitudes are significantly different, especially for P135+16 and P187–02, the objects with the largest separations. P135+16 is a radio-loud quasar with a radio-loudness parameter of $R = 91.4 \pm 8.8$ (Bañados et al. 2015b). However, if instead of the *WISE* photometry the *Spitzer* photometry is used as a proxy for the optical luminosity, the radio-loudness parameter increases to $R = 229.9 \pm 11.7$, making P135+16 the radio-loudest quasar at $z > 5.5$ (see Figure 2 in Bañados et al. 2015b). Based on Figure 14 and the discrepancies between the *WISE* and *Spitzer* photometry, we include in Figure 5 only objects with a separation between the *WISE* and optical/near-infrared coordinates that is smaller than 2″.

Figure 15 shows the *WISE* magnitudes and colors for the 111 (∼65%) known $z > 5.6$ quasars that are detected in at least one

Table 9
Candidates Spectroscopically Confirmed to *not* be $z > 5.6$ Quasars

Rejected Candidate	R.A. J2000	Decl. J2000	i_{P1} (mag)	z_{P1} (mag)	y_{P1} (mag)	Y (mag)	J (mag)	$E(B-V)$ (mag)	PS1 [a]
P014+37	00:56:09.20	+37:34:16.1	23.07 ± 0.24	20.50 ± 0.05	19.88 ± 0.06	19.46 ± 0.18	19.00 ± 0.08	0.05	2
P023+30	01:32:42.94	+30:49:30.1	21.87 ± 0.08	19.14 ± 0.01	19.39 ± 0.04	⋯	⋯	0.05	1
P102+55	06:49:07.97	+55:35:25.8	>23.57	21.07 ± 0.09	19.25 ± 0.03	20.23 ± 0.06	20.14 ± 0.04	0.06	3
P116–07	07:44:13.22	−07:46:22.2	22.10 ± 0.19	20.07 ± 0.04	19.70 ± 0.06	⋯	19.43 ± 0.07	0.16	1
P131+25	08:47:45.26	+25:47:17.3	>23.69	21.39 ± 0.09	20.67 ± 0.13	20.55 ± 0.16	20.06 ± 0.09	0.04	2
P150+16	10:03:39.37	+16:05:31.0	23.69 ± 0.36	21.30 ± 0.07	20.85 ± 0.11	⋯	19.90 ± 0.11	0.04	1
P165+25	11:02:23.27	+25:39:35.8	22.90 ± 0.23	20.89 ± 0.06	19.85 ± 0.07	⋯	19.55 ± 0.09	0.02	2
P215+33	14:22:16.12	+33:29:21.3	23.19 ± 0.20	20.55 ± 0.04	19.56 ± 0.03	⋯	19.16 ± 0.09	0.01	2
P242+75	16:09:32.85	+75:10:58.8	>22.67	>22.41	20.23 ± 0.13	19.40 ± 0.03	19.01 ± 0.04	0.03	3
P274+45	18:18:19.95	+45:38:49.8	>23.94	21.50 ± 0.10	20.62 ± 0.12	⋯	20.29 ± 0.20	0.04	2
P352+35	23:29:03.78	+35:30:27.3	21.94 ± 0.19	19.82 ± 0.02	19.69 ± 0.06	⋯	19.26 ± 0.06	0.10	1

Note.
[a] PS1 criteria: 0—None; 1—Criteria of Section 2.1.1 with $z_{P1} - y_{P1} < 0.5$; 2—Criteria of Section 2.1.1 with $z_{P1} - y_{P1} \geqslant 0.5$; 3—Criteria of Venemans et al. (2015a).

of the *WISE* bands with S/N > 3. The dashed lines show the nominal 5σ ALLWISE limiting magnitudes, but there are regions of the sky that reach significantly greater magnitudes. The dotted line represents the expected median 5σ limiting magnitude once the data from ALLWISE are combined with the ongoing NEOWISE reactivated mission (Mainzer et al. 2014), which is surveying the sky in *W*1 and *W*2 to search for near-Earth objects. This increase in depth will also be beneficial to efficiently searching for the brightest quasars at the highest accessible redshifts ($\gtrsim 7$).

Table 8 presents the *WISE*, *J*-band, and PS1 PV3 magnitudes of the 173 $z > 5.6$ quasars known by 2016 March. Almost 81% (140/173) of the known $z > 5.6$ quasars are detected in at least one of the PS1 bands with S/N > 5, while a similar fraction (141/173) have *J*-band information with S/N > 5. There are seven known quasars with decl. $< -30°$, which are therefore outside the PS1 footprint.

APPENDIX C
SPECTROSCOPICALLY REJECTED CANDIDATES

Table 9 presents the 11 candidates whose spectra showed they were not $z > 5.6$ quasars. Objects with a PS1 value of 1 are mostly M and L dwarfs, while sources with a PS1 value of 2 or 3 are more likely to be late L dwarfs and T dwarfs. However, a thorough classification of these objects is beyond the scope of this work.

REFERENCES

Alam, S., Albareti, F. D., Allende Prieto, C., et al. 2015, ApJS, 219, 12
Appenzeller, I., & Rupprecht, G. 1992, Msngr, 67, 18
Arp, H. C., Bolton, J. G., & Kinman, T. D. 1967, ApJ, 147, 840
Astropy Collaboration, Robitaille, T. P., Tollerud, E. J., et al. 2013, A&A, 558, A33
Bailer-Jones, C. A., Bizenberger, P., & Storz, C. 2000, Proc. SPIE, 4008, 1305
Bañados, E., Decarli, R., Walter, F., et al. 2015a, ApJL, 805, L8
Bañados, E., Venemans, B. P., Morganson, E., et al. 2014, AJ, 148, 14
Bañados, E., Venemans, B. P., Morganson, E., et al. 2015b, ApJ, 804, 118
Barnett, R., Warren, S. J., Banerji, M., et al. 2015, A&A, 575, A31
Becker, G. D., Bolton, J. S., & Lidz, A. 2015a, PASA, 32, e045
Becker, G. D., Bolton, J. S., Madau, P., et al. 2015b, MNRAS, 447, 3402
Becker, R. H., White, R. L., & Helfand, D. J. 1995, ApJ, 450, 559
Best, W. M. J., Liu, M. C., Magnier, E. A., et al. 2015, ApJ, 814, 118
Bizenberger, P., McCaughrean, M. J., Birk, C., Thompson, D., & Storz, C. 1998, Proc. SPIE, 3354, 825
Blain, A. W., Assef, R., Stern, D., et al. 2013, ApJ, 778, 113
Brown, W. R., McLeod, B. A., Geary, J. C., & Bowsher, E. C. 2008, Proc. SPIE, 7014, 2
Buzzoni, B., Delabre, B., Dekker, H., et al. 1984, Msngr, 38, 9
Calura, F., Gilli, R., Vignali, C., et al. 2014, MNRAS, 438, 2765
Carilli, C. L., Neri, R., Wang, R., et al. 2007, ApJL, 666, L9
Carilli, C. L., Wang, R., Fan, X., et al. 2010, ApJ, 714, 834
Carnall, A. C., Shanks, T., Chehade, B., et al. 2015, MNRAS, 451, L16
Casali, M., Adamson, A., Alves de Oliveira, C., et al. 2007, A&A, 467, 777
Cool, R. J., Kochanek, C. S., Eisenstein, D. J., et al. 2006, AJ, 132, 823
Cutri, R. M. 2012, yCat, 2311, 0
Cutri, R. M. 2014, yCat, 2328, 0
De Rosa, G., Decarli, R., Walter, F., et al. 2011, ApJ, 739, 56
De Rosa, G., Venemans, B. P., Decarli, R., et al. 2014, ApJ, 790, 145
Diamond-Stanic, A. M., Fan, X., Brandt, W. N., et al. 2009, ApJ, 699, 782
Fan, X., Hennawi, J. F., Richards, G. T., et al. 2004, AJ, 128, 515
Fan, X., Narayanan, V. K., Lupton, R. H., et al. 2001, AJ, 122, 2833
Fan, X., Strauss, M. A., Richards, G. T., et al. 2006, AJ, 131, 1203
Fan, X., Strauss, M. A., Schneider, D. P., et al. 2003, AJ, 125, 1649
Fan, X., White, R. L., Davis, M., et al. 2000, AJ, 120, 1167
Goto, T. 2006, MNRAS, 371, 769
Greiner, J., Bornemann, W., Clemens, C., et al. 2008, PASP, 120, 405
Hambly, N. C., Collins, R. S., Cross, N. J. G., et al. 2008, MNRAS, 384, 637
Hamuy, M., Folatelli, G., Morrell, N. I., et al. 2006, PASP, 118, 2
Hewett, P. C., Warren, S. J., Leggett, S. K., & Hodgkin, S. T. 2006, MNRAS, 367, 454
Hunter, J. D. 2007, CSE, 9, 90
Jiang, L., Fan, X., Annis, J., et al. 2008, AJ, 135, 1057
Jiang, L., Fan, X., Bian, F., et al. 2009, AJ, 138, 305
Jiang, L., McGreer, I. D., Fan, X., et al. 2015, AJ, 149, 188
Jiang, L., McGreer, I. D., Fan, X., et al. 2016, ApJ, in press (arXiv:1610.05369)
Kaiser, N., Aussel, H., Burke, B. E., et al. 2002, Proc. SPIE, 4836, 154
Kaiser, N., Burgett, W., Chambers, K., et al. 2010, Proc. SPIE, 7733, 12
Kashikawa, N., Ishizaki, Y., Willott, C. J., et al. 2015, ApJ, 798, 28
Kim, Y., Im, M., Jeon, Y., et al. 2015, ApJL, 813, L35
Kurk, J. D., Walter, F., Fan, X., et al. 2007, ApJ, 669, 32
Kurk, J. D., Walter, F., Fan, X., et al. 2009, ApJ, 702, 833
Laor, A., & Davis, S. W. 2011, MNRAS, 417, 681
Lawrence, A., Warren, S. J., Almaini, O., et al. 2007, MNRAS, 379, 1599
Leipski, C., Meisenheimer, K., Walter, F., et al. 2014, ApJ, 785, 154
Liu, Y., & Zhang, S. N. 2011, ApJL, 728, L44
Lodieu, N., Boudreault, S., & Béjar, V. J. S. 2014, MNRAS, 445, 3908
Luo, B., Brandt, W. N., Hall, P. B., et al. 2015, ApJ, 805, 122
Mace, G. N. 2014, PhD thesis, Univ. California Los Angeles
Magnier, E. 2006, in The Advanced Maui Optical and Space Surveillance Technologies Conf., ed. D. B. Ryan (Maui, HI: Maui Economic Development Board), E50
Magnier, E. 2007, in ASP Conf. Ser. 364, The Future of Photometric, Spectrophotometric and Polarimetric Standardization, ed. C. Sterken (San Francisco, CA: ASP), 153
Mahabal, A., Stern, D., Bogosavljević, M., Djorgovski, S. G., & Thompson, D. 2005, ApJL, 634, L9
Mainzer, A., Bauer, J., Cutri, R. M., et al. 2014, ApJ, 792, 30

Marocco, F., Jones, H. R. A., Day-Jones, A. C., et al. 2015, MNRAS, 449, 3651
Matsuoka, Y., Onoue, M., Kashikawa, N., et al. 2016, ApJ, 828, 26
McGreer, I. D., Becker, R. H., Helfand, D. J., & White, R. L. 2006, ApJ, 652, 157
McGreer, I. D., Jiang, L., Fan, X., et al. 2013, ApJ, 768, 105
McMahon, R. G., Banerji, M., Gonzalez, E., et al. 2013, Msngr, 154, 35
Moorwood, A., Cuby, J.-G., & Lidman, C. 1998, Msngr, 91, 9
Morganson, E., De Rosa, G., Decarli, R., et al. 2012, AJ, 143, 142
Mortlock, D. J. 2015, arXiv:1511.01107
Mortlock, D. J., Patel, M., Warren, S. J., et al. 2009, A&A, 505, 97
Mortlock, D. J., Warren, S. J., Venemans, B. P., et al. 2011, Natur, 474, 616
Oke, J. B., Cohen, J. G., Carr, M., et al. 1995, PASP, 107, 375
Oke, J. B., & Gunn, J. E. 1982, PASP, 94, 586
Pâris, I., Petitjean, P., Aubourg, É., et al. 2014, A&A, 563, A54
Planck Collaboration, Ade, P. A. R., Aghanim, N., et al. 2016, A&A, 594, A13
Plotkin, R. M., Shemmer, O., Trakhtenbrot, B., et al. 2015, ApJ, 805, 123
Pogge, R. W., Atwood, B., Brewer, D. F., et al. 2010, Proc. SPIE, 7735, 9
Reed, S. L., McMahon, R. G., Banerji, M., et al. 2015, MNRAS, 454, 3952
Richards, G. T., Vanden Berk, D. E., Reichard, T. A., et al. 2002, AJ, 124, 1
Schlafly, E. F., & Finkbeiner, D. P. 2011, ApJ, 737, 103
Schlegel, D. J., Finkbeiner, D. P., & Davis, M. 1998, ApJ, 500, 525
Schmidt, G. D., Weymann, R. J., & Foltz, C. B. 1989, PASP, 101, 713
Schmidt, M. 1963, Natur, 197, 1040
Schmidt, M. 1965, ApJ, 141, 1295
Seifert, W., Appenzeller, I., Baumeister, H., et al. 2003, Proc. SPIE, 4841, 962
Selsing, J., Fynbo, J. P. U., Christensen, L., & Krogager, J.-K. 2016, A&A, 585, A87
Shemmer, O., & Lieber, S. 2015, ApJ, 805, 124
Shen, Y., Brandt, W. N., Denney, K. D., et al. 2016, arXiv:1602.03894
Simcoe, R. A., Burgasser, A. J., Bernstein, R. A., et al. 2008, Proc. SPIE, 7014, 27
Simcoe, R. A., Burgasser, A. J., Schechter, P. L., et al. 2013, PASP, 125, 270
Simpson, C., Mortlock, D., Warren, S., et al. 2014, MNRAS, 442, 3454
Skrutskie, M. F., Cutri, R. M., Stiening, R., et al. 2006, AJ, 131, 1163
Stern, D., Kirkpatrick, J. D., Allen, L. E., et al. 2007, ApJ, 663, 677
Tonry, J. L., Stubbs, C. W., Lykke, K. R., et al. 2012, ApJ, 750, 99
Vanden Berk, D. E., Richards, G. T., Bauer, A., et al. 2001, AJ, 122, 549
Venemans, B. P., Bañados, E., Decarli, R., et al. 2015a, ApJL, 801, L11
Venemans, B. P., Findlay, J. R., Sutherland, W. J., et al. 2013, ApJ, 779, 24
Venemans, B. P., McMahon, R. G., Walter, F., et al. 2012, ApJL, 751, L25
Venemans, B. P., McMahon, R. G., Warren, S. J., et al. 2007, MNRAS, 376, L76
Venemans, B. P., Verdoes Kleijn, G. A., Mwebaze, J., et al. 2015b, MNRAS, 453, 2259
Venemans, B. P., Walter, F., Zschaechner, L., et al. 2016, ApJ, 816, 37
Volonteri, M. 2012, Sci, 337, 544
Wang, F., Wu, X.-B., Fan, X., et al. 2016a, ApJ, 819, 24
Wang, J.-M., Qiu, J., Du, P., & Ho, L. C. 2014, ApJ, 797, 65
Wang, R., Carilli, C. L., Neri, R., et al. 2010, ApJ, 714, 699
Wang, R., Carilli, C. L., Wagg, J., et al. 2008, ApJ, 687, 848
Wang, R., Wagg, J., Carilli, C. L., et al. 2011, ApJL, 739, L34
Wang, R., Wagg, J., Carilli, C. L., et al. 2013, ApJ, 773, 44
Wang, R., Wu, X.-B., Neri, R., et al. 2016, ApJ, 830, 53
West, A. A., Morgan, D. P., Bochanski, J. J., et al. 2011, AJ, 141, 97
Willott, C. J., Albert, L., Arzoumanian, D., et al. 2010a, AJ, 140, 546
Willott, C. J., Bergeron, J., & Omont, A. 2015, ApJ, 801, 123
Willott, C. J., Delorme, P., Omont, A., et al. 2007, AJ, 134, 2435
Willott, C. J., Delorme, P., Reylé, C., et al. 2009, AJ, 137, 3541
Willott, C. J., Delorme, P., Reylé, C., et al. 2010b, AJ, 139, 906
Willott, C. J., Omont, A., & Bergeron, J. 2013, ApJ, 770, 13
Wright, E. L., Eisenhardt, P. R. M., Mainzer, A. K., et al. 2010, AJ, 140, 1868
Wu, J., Brandt, W. N., Anderson, S. F., et al. 2012, ApJ, 747, 10
Wu, X.-B., Wang, F., Fan, X., et al. 2015, Natur, 518, 512
Zeimann, G. R., White, R. L., Becker, R. H., et al. 2011, ApJ, 736, 57